

Large-Scale Dynamical Models and Estimation for Permeation in Biological Membrane Ion Channels

Modeling the ways that certain ions pass through, or are blocked by, ion channels is expected allow researchers to identify channel functions from their atomic structure.

By VIKRAM KRISHNAMURTHY, *Fellow IEEE*, AND SHIN-HO CHUNG

ABSTRACT | Biological ion channels are water-filled angstrom-unit (1 angstrom unit = 10^{-10} m) sized pores formed by proteins in the cell membrane. They are responsible for regulating the flow of ions into and out of a cell and hence they control all electrical activities in a cell. This paper deals with constructing large scale stochastic dynamical models for explaining ion permeation; that is, how individual ions interact with the protein atoms in an ion channel and travel through the channel. These permeation models capture the dynamics of the ions at a femto-second time scale and angstrom-unit spatial scale. We review large scale multiparticle simulation methods such as Brownian dynamics for modeling permeation. Then we present a novel multiparticle simulation methodology, which we call adaptive controlled Brownian dynamics, for estimating the force experienced by a permeating ion at each discrete position along the ion-conducting pathway. The profile of this force, commonly known as the *potential of mean force*, results from the electrostatic interactions between the ions in the conduit and all the charges carried by atoms forming the channel the protein, as well as the induced charges on the protein wall. We illustrate the use of adaptive controlled Brownian dynamics in gramicidin channels and shape estimation of sodium channels.

KEYWORDS | Adaptive controlled Brownian dynamics (ACBD); biological ion channels; permeation; stochastic optimization

I. INTRODUCTION

All living cells are surrounded by a thin cell membrane, which is composed of two layers of phospholipid molecules. The cell membrane acts as a hydrophobic, low dielectric barrier that is impermeable to charged particles such as Na^+ , K^+ , Cl^- ions. Indeed, the amount of energy needed to transport one monovalent ion across the cell membrane is insurmountably high—this energy called the Born energy is about 65 kT.¹

So how do ions diffuse in and out of a cell? The transport of ions across the cell membrane is regulated by specialized water-filled conduits called *ion channels*. Ion channels are biological subnanotubes formed by protein molecules across the cell membrane through which ions can freely move in and out when the gates are open. These ion channels have typical pore diameters of $\sim 10^{-9}$ m or 10 Å.

Ion channels in cell membranes play a crucial role in all living organisms. They regulate all electrical activities in the nervous system, including communication between cells and the influence of hormones and drugs on cell function. Because ion channels are elementary building blocks of brain function, understanding their mechanisms

Manuscript received October 1, 2006; revised January 23, 2007. This work was supported by NSERC.

V. Krishnamurthy is with the Department of Electrical and Computer Engineering, University of British Columbia, Vancouver V6T 1Z4, Canada (e-mail: vikramk@ece.ubc.ca).

S.-H. Chung is with the Australian National University, Canberra ACT 0200, Australia (e-mail: shin-ho.chung@anu.edu.au).

Digital Object Identifier: 10.1109/JPROC.2007.893246

¹The unit kT is widely used for measuring energy. Here, $k = 1.38 \times 10^{-23}$ J/T denotes the Boltzmann constant and T denotes the absolute temperature.

at a molecular level is a fundamental problem in biophysics. A remarkable property of ion channels is that they are selectively conductive. For example, sodium (Na) channels primarily allow sodium ions to permeate but do not allow significant amounts of other types of ions such as potassium or calcium ions. Several inherited neurological, muscular, and renal disorders arise from malfunctioning of ion channels. Examples of ion channel diseases include (see [1] for details): *hyperkalaemic muscle paralysis* that can result from malfunctioning of muscular Na channels; *epilepsy* with febrile seizure, caused sometimes by the abnormality of neuronal Na channels; *migraines*, believed to be a neuronal calcium (Ca) channel disease; and *polycystic kidney disorder* that arises from a mutation of the Ca channel. In addition, genetic alteration of the proteins forming chloride channels are known to be associated with *cystic fibrosis* which is a fatal pancreatic and lung disease, *Bartter's syndrome* which is a salt-wasting renal tubular disorder, and *diabetes*. Thus, the elucidation of how single channels work will ultimately help find the causes of, and potentially cures for, a number of inherited disorders. We refer the reader to the special issue [2] and the recent book [3] for a detailed exposition of recent results in ion channels written by several leading researchers in the area. Also [4] is a classic exposition on ion channels.

This paper deals with ion channel permeation. The *permeation problem* [5], [6] seeks to explain the working of an ion channel at an angstrom ($1 \text{ \AA} = 10^{-10} \text{ m}$) spatial scale by studying the propagation of individual ions through the ion channel at a femto-second (10^{-15}) time scale. In the past few years, there have been enormous strides in our understanding of the structure–function relationships in biological ion channels due to the combined efforts of experimental and computational biophysicists. In recent breakthroughs, the crystal structures of the potassium channels, mechanosensitive channel, chloride channel, and nicotinic acetylcholine receptor have been determined from crystallographic analysis [7]–[13]. The 2003 Nobel prize in chemistry was awarded to R. MacKinnon for determining the crystallographic structures of several different ion channels including the bacterial potassium channel.² It is expected that crystal structures of other ion channels will follow these discoveries, ushering in a new era in ion channel studies, where predicting function of channels from their atomic structures will become the main quest. Parallel to these landmark experimental findings, there have also been important advances in computational biophysics. As new analytical methods have been developed and the available

computational power increased, theoretical models of ion permeation have become increasingly sophisticated. It has now become possible to relate the atomic structure of an ion channel to its function through the fundamental laws of physics operating in electrolyte solutions. Many aspects of macroscopic observable properties of ion channels are being addressed by molecular and stochastic dynamics simulations. Quantitative statements based on rigorous physical laws are replacing qualitative explanations of how ions permeate across narrow pores formed by the protein wall and how ion channels allow one ionic species to pass while blocking others. The computational methods of solving complex biological problems, such as permeation, selectivity, and gating mechanisms of ion channels, will increasingly play prominent roles as the speed of computers increases and theoretical approaches that are currently under development become refined further.

This paper highlights the ubiquitous nature of large scale stochastic dynamical systems and their estimation and control. Ion channel permeation is modeled as a large scale multiparticle stochastic dynamical system comprising several ions and water molecules that interact with the protein atoms lining the inner wall of the ion channel. We also show how stochastic optimization algorithms can be used to estimate certain structural parameters of the ion channel. The paper has the following main contributions.

- 1) In Section II, we give a brief account of several different computational tools employed to study the mechanisms of ion permeation across biological ion channels. These are: *ab initio* and classical molecular dynamics, Brownian dynamics (BD), Poisson–Nernst–Planck (PNP) theory, and reaction rate theory. The merits and shortcomings of each of these approaches are discussed in detail in several recent publications, to which the reader is referred [4], [14]–[18].
- 2) Section III gives a detailed stochastic dynamical formulation of BD in terms of a large scale multiparticle system with dynamics evolving according to the Langevin equation. The various forces acting on the ion due to other ions and the protein atoms lining the ion channel are formulated. A probabilistic interpretation of BD simulation in terms of mean first passage times is also given.
- 3) In Section IV, we show how BD simulations can be used to explain ion permeation in three important types of ion channels namely, potassium channels, CLC chloride channels, and calcium channels. We describe how BD simulations can replicate the macroscopic current–voltage–concentration behavior of ion channels.
- 4) In Section V, we describe a novel stochastic optimization framework for dynamically controlling BD simulation to estimate the potential of mean force (PMF) of a gramicidin ion channel and the shape of a sodium channel. We formulate these

²The 2003 Nobel prize in Chemistry Press Release reads: “Roderick MacKinnon surprised the whole research community when in 1998 he was able to determine the spatial structure of a potassium channel. Thanks to this contribution we can now see ions flowing through channels that can be opened and closed by different cellular signals. . . The ion channels are important for, among other things, the function of the nervous system and the muscles.”

estimation problems as stochastic optimization problems. In Section VI, we give several stochastic optimization algorithms to estimate these parameters. We call these adaptive controlled Brownian dynamics (ACBD) algorithms [19], [20]. These stochastic optimization algorithms are implemented as stochastic approximation algorithms that dynamically control the behavior of the BD simulation. Several novel discrete stochastic approximation algorithms are presented together with a kernel-based exploration-exploitation algorithm. We present numerical examples implemented on a multiprocessor supercomputer to illustrate the ACBD algorithms for estimating the PMF of gramicidin and shape of sodium channels.

II. LEVELS OF ABSTRACTION FOR PERMEATION MODELING IN ION CHANNELS

This section outlines four levels of abstraction that have been widely used to model permeation in ion channels. The section sets the stage for BD modeling for permeation which is the main focus of the paper.

A fundamental goal in biophysics is to construct accurate dynamical models for ion permeation in biological ion channels. Such models link channel structure (which is typically defined in terms of an atomic model at the subnanoscale) to channel function (which is observed via experimental measurements at the macroscopic time scale). Any high-resolution dynamical model for ion permeation needs to consider three ingredients: the ions, water molecules, and the atoms of the protein that form the ion channel. It is essential for such dynamical models to be based on physical principles and to result in computationally tractable simulation algorithms. Such models also need to elucidate the detailed mechanisms of ion permeation—where the binding sites are in the channel, how fast an ion moves from one binding site to another, and where the rate-limiting steps are in conduction. Finally, it will make predictions that can be confirmed or refuted experimentally.

The computational tools of physics employed in this endeavor, from fundamental to phenomenological, are *ab initio* and classical molecular dynamics, Brownian dynamics, continuum theories, and reaction rate theory. These approaches make various levels of abstractions in replacing the complex reality with a model, the system composed of channel macromolecules, lipid bilayer, ions, and water molecules. Each of these approaches has its strengths and limitations and involves a degree of approximation.

Ab Initio Quantum Mechanical Models: At the lowest level of abstraction, we have the *ab initio* quantum mechanical approach, in which the interactions between the ions, water molecules, and protein atoms are determined

from first-principle electronic structure calculations by solving the many-body Schrödinger equation. There are three terms in the Hamiltonian: the nuclear part, electronic part, and the Coulomb interaction between them [21]. As there are no free parameters in this approach, it represents the ultimate tool to the modeling of biomolecular systems. Because a solution of the Schrödinger equation is formidable and is an extremely time-consuming process, even with some simplifying assumptions, its applications are limited to very small systems at present.

Molecular Dynamics (MD): By replacing the potential energy featuring in the many-body quantum mechanical equation with a phenomenological one, a purely classical description of a system can be obtained. This is called classical MD [22]. MD simulations are carried out using empirically determined pair-wise interaction potentials between the ions, water molecules, and protein atoms, and their trajectories are followed using Newton's equation of motion. Although it is possible to model an entire ion channel in this way, it is not computationally tractable to simulate molecular dynamics long enough to see permeation of ions across an ion channel and to determine its conductance, which is the most important channel property. Note, however, that molecular dynamics is widely used to understand how the ions and protein of the ion channel interact over small segments of the ion channel. Indeed, MD is used to compute the potential of mean force (PMF), which represents the forces an ion encounters due to the protein that forms the ion channel [23] (we give a more detailed exposition of the PMF and how to estimate it in Section V). The resulting PMF is used conjunction with Brownian dynamics, described as follows.

BD: The precise formulation of BD, which is the main focus of the paper, is given in Section III. Here, we briefly provide a comparison of BD with the other methodologies particularly, MD and Poisson–Nernst–Planck (PNP) theory.

Unlike MD, with BD it is computationally tractable to run a computer simulation to see permeation of ions across the ion channel. For this reason, BD constitutes an engineering viable model for permeation. Using BD, one can simulate channel conductances under various conditions and compare these simulated results with experimental observations with only a modest amount of computational power. This ability to compute current flow across ion channels confers a distinct advantage to BD compared to simulation techniques. To trace the trajectories of about 100 ions interacting with a dielectric boundary for many microseconds, a period long enough to deduce the conductance of an ion channel, BD makes two simplifying assumptions compared to MD.

- 1) First, water is not treated explicitly but as a continuum. Water molecules that form the bulk of the system in ion channels are integrated out and only

the ions themselves are explicitly simulated. The net effects of incessant collisions between ions and water molecules are lumped together and treated as the frictional and random forces. This treatment of explicit water molecules by implicit water can be viewed as a functional central limit theorem approximation.

- 2) Second, the atoms in the protein that form the ion channel are considered to be fixed, whereas in reality they will undergo rapid thermal fluctuations. Several independent lines of evidence suggest that root-mean-square (rms) fluctuations of typical proteins are of the order of 0.75 Å, suggesting that the transmembrane passage through which ions traverse may be quite flexible [24], [25]. The fixed protein assumption can be explained via stochastic averaging theory. We may construe that the dynamics of ion channel is composed of two parts: protein fluctuations that occur at the fast time scale and movement of ions across the pore that occur at the slower time scale. Then, stochastic averaging theory says that the parts of the system moving on the fast time scale (namely, the protein) will perceive the slowly moving portions (namely, the ions) as constant and the slowly moving portions (ions) only see a time-averaged effect from the fast time scale parts (protein). We refer the reader to [26] and [27] for an extensive treatment of stochastic averaging theory. Stochastic averaging theory is widely used to analyze the convergence of adaptive filters in statistical signal processing [28].

PNP Theory: A still higher level of abstraction is the PNP theory [29]–[32], which is based on the continuum hypothesis of electrostatics. In this and other electrodiffusion theories, one makes a further simplification, known as the mean-field approximation. In this approach, ions are treated not as discrete entities but as continuous charge densities that represent the space-time average of the microscopic motion of ions. In the PNP theory, the flux of an ionic species is described by the Nernst–Planck equation that combines Ohm’s law with Fick’s law of diffusion, and the potential at each position is determined from the solution of Poisson’s equation using the total charge density (ions plus fixed charges). The PNP theory thus incorporates the channel structure, and its solution yields the potential, concentration, and flux of ions in the system in a self-consistent manner.

Reaction Rate Theory: Finally, there is one other approach that has been employed to model biological ion channels, namely, the reaction rate theory [4], [33]. In this approach, an ion channel is represented by a series of ion binding sites separated by barriers, and ions are assumed to hop from one binding site to another, with the probability of

each hop determined by the height of the energy barrier. Although the model parameters have no direct physical relation to the channel structure, many useful insights have been gleaned in the past about ion permeation using this approach.

Several comprehensive recent review articles give detailed expositions of each of these approaches. As the primary focus of this paper is BD, these other approaches are not discussed further here. Instead, for details, the reader is referred to [3], [18], and [21]. We also refer the reader to [34], where a novel birth–death Markov chain is used to model permeation.

A. Discussion

The three computational tools discussed in this section, namely PNP theory, MD, and BD, play important roles in understanding ion channel permeation. Each of these approaches has its strengths and limitations and involves a degree of approximation. The main defects of PNP are errors stemming from the mean-field assumption. In particular, it ignores the effects of induced surface charges created as a charged particle in electrolyte solutions approaches the protein boundary. The magnitude of the errors introduced by the mean-field approximation become large when the theory is applied to narrow ion channels. By incorporating a term in the PNP equations to account for the barrier created by induced surface charges, the magnitude of the errors can be reduced somewhat. However, doing this removes much of the simplicity of the theory, one of its main advantages over the other approaches, and also it is still hard to know the accuracy of the results without comparison to a more detailed model.

The greatest limitation of MD is its prohibitive computational cost. This computational cost limits the time horizon over which an ion permeation simulation can be carried out. While the calculation of free energy profiles provides useful information on ion permeation, it is not a substitute for a direct estimation of conductance from simulations. Thus, virtually no predictions derived from molecular dynamics simulations can be directly compared with experimental data. If no such comparisons can be made, there can only be a limited interaction between experimenters and theoreticians. With the current doubling of computer speeds every two years, this computational limitation will eventually be overcome. Then, the force fields employed in molecular dynamics simulations may need to be improved to include polarization effects, perhaps using *ab initio* molecular dynamics as a guide.

One of the main caveats to the application of BD to biological ion channels is the use of the macroscopic (bulk) Poisson’s equation (7) to estimate the forces encountered by permeating ions—see Section III-C. The issue here is whether one can legitimately employ macroscopic electrostatics in regions that are not much larger than the diameters of the water molecules and ions. In the narrow constricted region of the channel, such as a gramicidin

channel or the selectivity filter of the potassium channel, the representation of the channel contents as a continuous medium is a poor approximation. A major focus of the rest of this paper (Section V and Section VI) is to overcome this limitation of BD by directly estimating the PMF via stochastic optimization algorithms.

MD, BD, and PNP approaches are useful in elucidating the mechanisms underlying selectivity and permeation of ions across biological ion channels. For ion channels with large pore radii, such as mechano-sensitive channels, PNP theory can be fruitfully utilized. Also, if one is interested in simply obtaining order-of-magnitude estimates of conductances of various model channels, this simple theory will provide the answers with little computational cost. To study the mechanisms underlying the selectivity sequences of monovalent ions or to determine the precise conformational changes of the protein when a channel undergoes the transition from the closed to the open state, one has to rely on MD simulations.

III. BD FORMULATION FOR ION PERMEATION

As described, BD offers a computationally tractable method for following the trajectories of interacting ions through an ion channel. In this section, we give a complete description of the BD dynamics and associated BD simulation algorithm for ion channel permeation. The main idea is to formulate BD as a multiparticle stochastic dynamical system comprising ions interacting with the protein atoms that form the ion channel. The reader should keep in mind that our eventual goal is to use BD to relate the atomic structure of the ion channel to its macroscopic behavior, i.e., the experimentally determined current-concentration-voltage behavior of the ion channel. By running BD simulations under different experimental conditions, one can compute current-voltage and conductance-concentration curves, which can be directly compared to the physiological measurements to assess the reliability and predictive power of the method. One can carry out a trajectory analysis of ions in the system to determine the steps involved in conduction such as the binding sites and the average number of ions in the channel, both of which are experimentally observable quantities. It is also possible to study the mechanisms of blocking of channels by larger molecules or other ion species.

This section is organized as follows. In Section III-A, the key BD system equations for evolution of the ions are presented. Section III-B outlines the BD simulation algorithm at a conceptual level. Section III-C gives a detailed description of all the forces acting on the ions that need to be considered in the BD simulation algorithm. Section III-D gives a probabilistic interpretation of BD in terms of mean first passage times of a diffusion. It shows that the BD algorithm can be viewed as a Monte Carlo

simulation algorithm for solving a boundary valued partial differential equation. Finally, in Section III-E, we discuss some of the limitations of BD.

A. BD Formulation

Fig. 1 shows a schematic illustration of a BD simulation assembly. An ion channel is placed at the center of the assembly. The positions in three-dimensional (3-D) space of all the atoms forming the channel are given by its X-ray crystallographic structure, and the charge on each atom is assigned. (For ion channels with known structure such as

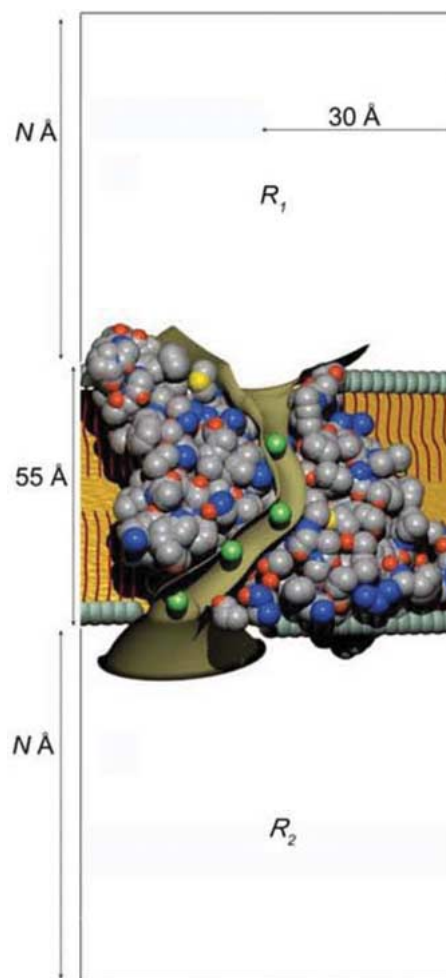


Fig. 1. BD simulation system for ion channel with complete atomic structure. Figure shows a CLC chloride channel imbedded in a lipid-bilayer is placed at the center of the simulation assembly and a large, cylindrical reservoir is attached at each end of the protein. Reservoirs are denoted as R_1 and R_2 . In the figure, front half of the atoms are removed to reveal ion-conducting pathway. Four Cl^- ions in the pore are shown in green. Uniform electric field is applied across the channel to mimic the membrane potential. This arrangement is equivalent to having two voltage plates far away from the channel.

gramicidin, CLC chloride channels, and KcsA potassium channels, the complete atomic structure can be downloaded from the protein data bank. The force field due to the fixed charges in the protein, see Section III-C, can then be obtained using a software package such as CHARMM (Chemistry at Harvard Macromolecular Mechanics) [35].

Then, two large cylindrical reservoirs \mathcal{R}_1 and \mathcal{R}_2 are attached to the ion channel \mathcal{C} as depicted in Fig. 1. These reservoirs mimic the extracellular and intracellular space. $2N$ ions are inserted into these reservoirs where N denotes a positive integer. These $2N$ ions are comprised of the following.

- 1) N positively charged ions indexed by $i = 1, 2, \dots, N$. Of these, $N/2$ ions indexed by $i = 1, 2, \dots, N/2$ are in \mathcal{R}_1 and $N/2$ ions indexed by $i = N/2 + 1, \dots, 2N$ are in \mathcal{R}_2 . Each positive ion has charge q^+ , mass $m^{(i)} = m^+$, frictional coefficient $m^+\gamma^+$, and radius r^+ . For example, a K^+ ion has charge $q^{(i)} = q^+ = 1.6 \times 10^{-19}$ C, mass $m^{(i)} = m^+ = 6.5 \times 10^{-26}$ kg and frictional coefficient $m^+\gamma^+$, where from the Einstein-Smoluchowski relation

$$m^+\gamma^+ = \frac{kT}{D}, \quad D = 1.96 \times 10^{-9} \text{ m}^2/\text{s}. \quad (1)$$

Here, $k = 1.38 \times 10^{-23}$ J/K denotes the Boltzmann constant and T denotes the temperature in Kelvin. K^+ ions have a radius $r^+ = 1.33$ Å.

- 2) N negatively charged ions. We index these by $i = N + 1, N + 2, \dots, 2N$. Of these, $N/2$ ions indexed by $i = N + 1, \dots, 3N/2$ are placed in \mathcal{R}_1 and the remaining $N/2$ ions indexed by $i = (3N/2) + 1, \dots, 2N$ are placed in \mathcal{R}_2 . Each negative ion has charge $q^{(i)} = q^-$, mass $m^{(i)} = m^-$, frictional coefficient $m^-\gamma^-$, and radius r^- . For example, a Cl^- ion has charge $q^{(i)} = q^- = -1.6 \times 10^{-19}$ C, mass $m^{(i)} = m^- = 5.9 \times 10^{-26}$ kg, and frictional coefficient $m^-\gamma^- = kT/D$ where $D = 2.03 \times 10^{-9}$ m/s². Cl^- ions have a radius $r^- = 1.81$ Å.

The membrane potential is imposed by applying a uniform electric field across the channel (Fig. 1). This is equivalent to placing a pair of large plates far away from the channel and applying a potential difference between them. Since the space between the voltage plates is filled with electrolyte solution, each reservoir is in iso-potential. That is, the average potential anywhere in the reservoir is identical to the applied potential at the voltage plate on that side, and the potential drop occurs almost entirely across the channel. Note that, as described in the following, the applied electric field is modified inside the channel by induced surface charges on the protein wall as well as fixed charges in the protein. The applied potential within the ion conducting pathway is highly nonuniform

with the largest changes occurring typically across narrowest segments.

Let $t \geq 0$ denote continuous time. Each ion j moves in 3-D space over time. Let $\mathbf{x}_t^{(i)} = (x_t^{(i)}, y_t^{(i)}, z_t^{(i)}) \in \mathcal{R}$ and $\mathbf{v}_t^{(i)} \in \mathbb{R}^3$ denote the position and velocity of ion i at time t . Let $\mathbf{X}_t = (\mathbf{x}_t^{(1)'}, \mathbf{x}_t^{(2)'}, \mathbf{x}_t^{(3)'}, \dots, \mathbf{x}_t^{(2N)'})'$ denote the positions and $\mathbf{V}_t = (\mathbf{v}_t^{(1)'}, \mathbf{v}_t^{(2)'}, \mathbf{v}_t^{(3)'}, \dots, \mathbf{v}_t^{(2N)'})'$ denote the velocities of all the $2N$ ions at time $t \geq 0$.

The algorithm for performing BD simulations is conceptually simple. The position and velocity of each individual ion evolves according to a continuous time stochastic dynamical system. The velocity of the ion with mass m and charge q located at a given position is determined by the force acting on it at time t . This velocity is computed by integrating the equation of motion, known as the *Langevin equation* (recall $i = 1, 2, \dots, N$ denote positive ions and $i = N + 1, \dots, 2N$ denote negative ions)

$$\mathbf{x}_t^{(i)} = \mathbf{x}_0^{(i)} + \int_0^t \mathbf{v}_s^{(i)} ds \quad (2)$$

$$m^\pm \mathbf{v}_t^{(i)} = m^\pm \mathbf{v}_0^{(i)} - \int_0^t m^\pm \gamma^\pm (\mathbf{x}_s^{(i)}) \mathbf{v}_s^{(i)} ds + \int_0^t F_\lambda^{(i)}(\mathbf{X}_s) ds + \int_0^t b^\pm (\mathbf{x}_s^{(i)}) d\mathbf{w}_s^{(i)}. \quad (3)$$

Here, $\gamma^\pm(\mathbf{x}_s^{(i)}) = \gamma^\pm$ (defined in the beginning of this section) if the ion is in the reservoir, and $\gamma(\mathbf{x}_s^{(i)})$ is determined by molecular dynamics simulation when the ion is in the ion channel [36]. The process $\{\mathbf{w}_t^{(i)}\}$ denotes a 3-D zero mean Brownian motion, which is component-wise independent. The constants b^+ and b^- are, respectively, $b^{+2}(\mathbf{x}_s^{(i)}) = 2m^+\gamma^+(\mathbf{x}_s^{(i)})kT$, $b^{-2}(\mathbf{x}_s^{(i)}) = 2m^-\gamma^-(\mathbf{x}_s^{(i)})kT$. The noise processes $\{\mathbf{w}_t^{(i)}\}$ and $\{\mathbf{w}_t^{(j)}\}$, that drive any two different ions, $j \neq i$, are assumed to be statistically independent.

The Langevin equation (3) is often written informally as

$$m^\pm \frac{d\mathbf{v}_t^{(i)}}{dt} = -m^\pm \gamma^\pm (\mathbf{x}_t^{(i)}) \mathbf{v}_t^{(i)} + F_\lambda^{(i)}(\mathbf{X}_t) + b^\pm (\mathbf{x}_t^{(i)}) \mathbf{e}_t^{(i)}$$

where $\mathbf{e}_t^{(i)}$ denotes continuous time white noise.

The above dynamics show that there are two main sources of the forces influencing the motion of ions in or in the vicinity of an ion channel that result in the ion channel current. These are the stochastic force and electric force. The former arises from the effects of collisions between ions and water molecules. Ions in electrolyte solutions are

tightly bound by shells of water molecules and these hydrated ions collide incessantly with surrounding water molecules. As a result of such bombardments, the motion of an ion is retarded by the friction term $m\gamma\mathbf{v}_t^{(i)}$, and it undergoes random fluctuations from an equilibrium position via the Brownian motion term $\mathbf{w}_t^{(i)}$. The term $F_\lambda(\cdot)$ in (3) models the systematic electrical forces acting on the ions when the external experimental condition is $\lambda \in \Lambda$ and is described in Section III-C.

Remark—Generalized Langevin Dynamics (GLD): A generalization of the above BD system called the GLD [37], [38] replaces γ in (3) with a time-varying friction kernel γ_t . The terms b^\pm depend on γ_t , and $m^\pm\gamma^+(\mathbf{x}_s^{(i)})\mathbf{v}_s^{(i)}ds$ in (3) is replaced with $m^\pm\gamma_{t-s}^\pm(\mathbf{x}_{t-s}^{(i)})\mathbf{v}_s^{(i)}ds$. In [37] and [38], γ_t is chosen as an exponentially decaying function of time t . It is concluded in [38] that GLD may be a more accurate model in regions of the ion channel where the energy barrier is present.

B. Brownian Dynamics Simulation Algorithm

To implement the BD simulation algorithm on a digital computer, it is necessary to discretize the continuous-time dynamical equation of the $2N$ ions (2), (3). There are several possible methods for time discretization of the stochastic differential equation (3), as described in detail by [39]. We used the second-order discretization described in [40]. In addition, to save computational resources, we used a two-time scale discretization in our simulations of the BD simulation algorithm. For dynamics of ions within the ion channel, the BD simulation algorithm uses a sampling interval of $\Delta = 2 \times 10^{-15}$ s. For dynamics of ions within the reservoirs a sampling interval of $\Delta = 2 \times 10^{-12}$ s is used in the reservoirs. The forces acting on each ion are calculated and the Langevin equation is used to determine where it will move in the next time step. By repeating this process many billions of times, usually for a simulation period lasting T time points (typically T is chosen in the order of $1 \mu\text{s}$), we can trace the movement of each ion in space during a simulation period and count how many ions have crossed the channel.

Denote the number of positive (respectively, negative) charges that cross from \mathcal{R}_1 to \mathcal{R}_2 over time T as $L_{\mathcal{R}_1, \mathcal{R}_2}^+$ (respectively, $L_{\mathcal{R}_1, \mathcal{R}_2}^-$). Also, denote the number of positive (respectively, negative) charges that cross from \mathcal{R}_2 to \mathcal{R}_1 as $L_{\mathcal{R}_2, \mathcal{R}_1}^+$ (respectively, $L_{\mathcal{R}_2, \mathcal{R}_1}^-$).

Algorithm 1 Brownian Dynamics Simulation Algorithm for ion permeation given experimental condition λ

- 1) Input experimental condition λ .
- 2) For T discrete time points, propagate all $2N$ ions according to the time discretized BD system (2), (3).

Each time an ion crosses the channel from reservoir \mathcal{R}_i to \mathcal{R}_j , $i, j \in \{1, 2\}$, uniformly pick an ion from \mathcal{R}_j and replace in \mathcal{R}_i .

- 3) Compute BD current estimate as

$$\hat{I}^{(\lambda)} = \frac{q^+}{T} \left(L_{\mathcal{R}_1, \mathcal{R}_2}^+ - L_{\mathcal{R}_2, \mathcal{R}_1}^+ \right) - \frac{q^-}{T} \left(L_{\mathcal{R}_1, \mathcal{R}_2}^- - L_{\mathcal{R}_2, \mathcal{R}_1}^- \right). \quad (4)$$

The sampling and replacement of ions in Algorithm 1 is required so that the concentration of ions in reservoirs \mathcal{R}_1 and \mathcal{R}_2 is approximately constant and equal to the desired experimental concentration specified by the experimental condition λ . Note that if the system was allowed to evolve for an infinite time without replacement, then eventually due to the external applied potential, more ions will be in \mathcal{R}_2 than \mathcal{R}_1 . This would violate the condition that the concentration of particles in \mathcal{R}_1 and \mathcal{R}_2 remains constant.

In [20], it is shown how the expected current $I^{(\lambda)} \triangleq \mathbf{E}\{\hat{I}^{(\lambda)}\}$ (where $\mathbf{E}\{\cdot\}$ denotes mathematical expectation) can be expressed in terms of the mean first passage times of ions crossing the ion channel. We briefly describe such a probabilistic construction in Section III-D. We show in Section III-D that these mean first passage times satisfy a boundary valued partial differential equation that is similar to the Kolmogorov equation. Strong consistency of the estimated current $\hat{I}^{(\lambda)}$ from the above BD algorithm can be established as shown in [20].

To carry out the above BD simulation algorithm for ion permeation through an ion channel, one needs to specify the boundaries of the system. This is a simple problem for 1-D BD simulations [41]–[43] but requires the addition of reservoirs to the channel system in the more realistic case of 3-D BD simulations. In several recent studies, a simple stochastic boundary has been used successfully in applications of BD simulations to a number of ion channels [14], [44], [45]. When an ion strikes the reservoir boundary during simulations, it is elastically scattered back into the reservoir, equivalent to letting an ion enter the reservoir whenever one leaves the simulation system. Thus, the concentrations of ions in the reservoirs are maintained at the desired values at all times. During simulations of current measurements, the chosen concentration values in the reservoirs are maintained by recycling ions from one side to the other whenever there is an imbalance due to a conduction event, mimicking the current flow through a closed circuit.

C. Systematic Force Acting on Ions

We now account for the various terms in the systematic force $F_\lambda(\cdot)$ in (3) acting on the ions in a BD formulation of

ion channel permeation. The systematic force experienced by each ion i is

$$F_{\lambda}^{(i)}(\mathbf{X}_t) = -q^{(i)} \nabla_{\mathbf{x}_t^{(i)}} \Phi_{\lambda}^{(i)}(\mathbf{X}_t)$$

where the scalar valued process $\Phi_{\lambda}^{(i)}(\mathbf{X}_t)$ denotes the total electric potential experienced by ion i given the position \mathbf{X}_t of all the $2N$ ions. We now give a detailed formulation of these systematic forces.

The potential $\Phi_{\lambda}^{(i)}(\mathbf{X}_t)$ experienced by each ion i is comprised of the following five components:

$$\begin{aligned} \Phi_{\lambda}^{(i)}(\mathbf{X}_t) = & U(\mathbf{x}_t^{(i)}) + \Phi_{\lambda}^{\text{ext}}(\mathbf{x}_t^{(i)}) + \Phi^{\text{IW}}(\mathbf{x}_t^{(i)}) \\ & + \Phi^{C,i}(\mathbf{X}_t) + \Phi^{\text{SR},i}(\mathbf{X}_t). \end{aligned} \quad (5)$$

The first three terms in (5), namely $U(\mathbf{x}_t^{(i)})$, $\Phi_{\lambda}^{\text{ext}}(\mathbf{x}_t^{(i)})$, $\Phi^{\text{IW}}(\mathbf{x}_t^{(i)})$ depend only on the position $\mathbf{x}_t^{(i)}$ of ion i , whereas the last two terms in (5) $\Phi^{C,i}(\mathbf{X}_t)$, $\Phi^{\text{SR},i}(\mathbf{X}_t)$ depend on the distance of ion i to all the other ions, namely, the position \mathbf{X}_t of all the ions. The five components in (5) are now defined.

- 1) *Potential of Mean Force (PMF)*, denoted $U(\mathbf{x}_t^{(i)})$ in (5), is comprised of electric forces acting on ion i when it is in or near the ion channel \mathcal{C} in Fig. 1. The PMF U originates from three different sources defined as follows and computation of the PMF requires solving three Poisson partial differential equations and adding the resulting solutions [which are potentials denoted $\phi(\cdot)$]. Poisson's equation relates the electric potential to the charge density. It reads³

$$\nabla(\epsilon(\mathbf{x}) \nabla \phi(\mathbf{x})) = -\frac{\rho(\mathbf{x})}{\epsilon_0}. \quad (6)$$

Here, $\phi(\cdot)$ denotes the potential and $\epsilon(\cdot)$ denotes the dielectric constant. Also, $\rho(\cdot)$ denotes the charge density and $\epsilon_0 \approx 8.85 \times 10^{-12}$ farad per meter is the permittivity of free space. We then make the assumption that the space is divided into two regions, water and protein, with $\epsilon_{\text{water}} = 80$ in water and $\epsilon_{\text{protein}} = 2$ in protein. This implies that

³It is interesting to note that the so-called self-consistent approximation [46] used to evaluate the current voltage response of a Carbon nanotube involves solving Poisson's equation coupled with Schrödinger's equation. In comparison, BD for ion permeation requires solving Poisson's equation (7) coupled with the Langevin equation (2), (3) which is distributionally equivalent to the Fokker-Planck equation.

in each region, (6) can be expressed as the macroscopic Poisson equation

$$\nabla^2 \phi(\mathbf{x}) = \frac{\rho(\mathbf{x})}{\epsilon_{\text{protein/water}} \times \epsilon_0} \quad (7)$$

subject to a boundary condition that the potential $\phi(\cdot)$ is continuous at the dielectric boundary and $\epsilon_{\text{water}} \nabla \phi'_{\text{water}} \hat{n} = \epsilon_{\text{protein}} \nabla \phi'_{\text{protein}} \hat{n}$, where \hat{n} is a unit normal to the surface. Unlike (6), (7) is no longer a fundamental equation, but rather a macroscopic (bulk) approximation (we discuss this further in Section III-E). The PMF U is computed as the sum of the solutions (potentials) of the following three Poisson equations.

- a) *Fixed Charges in Protein*: First, there are charges in the channel protein and the electric field emanating from them renders the pore attractive to one ionic species and repulsive to another. Because this is independent of the of ions, the potential $\phi(x)$ in (7) does not change during simulations. Thus, Poisson's equation can be solved numerically on a spatial grid in the absence of ions and the results stored on a 3-D lookup table.
- b) *Induced Surface Charges*: When any ion in the assembly comes near the protein wall, it induces surface charges of the same polarity at the water-protein interface. These are known as the induced surface charges. To compute this potential, Poisson's equation (7) is solved for a single ion with the external applied field and fixed charges switched off. The ion is moved through a spatial grid of points and the calculated self potentials are stored in a 3-D lookup table. If the channel boundary is axially symmetric, then a 2-D table suffices.
- c) *Reaction Potential*: Finally, the reaction potential needs to be taken into account. This is potential due to charges induced by an ion j when another ion i is kept at a fixed position. The computation is similar to that of the induced surface charges above. However, since the solution to Poisson's equation (7) contains the Coulomb and self potentials with respect to ion i , these need to be subtracted from the solution. The results can then be precomputed and stored in a 6-D table. For an axially symmetric channel, a 5-D table suffices.

- 2) *External Applied Potential*: In the vicinity of living cells, there is a strong electric field resulting from the membrane potential, which is generated by diffuse, unpaired, ionic clouds on each side of the

membrane. Typically, this resting potential across a cell membrane, whose thickness is about 50 Å, is 70 mV, the cell interior being negative with respect to the extracellular space.

For ion i at position $\mathbf{x}_t^{(i)} = (x, y, z)$, $\Phi_\lambda^{\text{ext}}(\mathbf{x}) = -\lambda z$ denotes the potential on ion i due to the applied external field. The electrical field acting on each ion due to the applied potential is therefore $-\nabla_{\mathbf{x}_t^{(i)}} \Phi_\lambda^{\text{ext}} = (0, 0, \lambda)$ V/m at all $\mathbf{x} \in \mathcal{R}$. It is this applied external field that causes a drift of ions from the reservoir \mathcal{R}_1 to \mathcal{R}_2 via the ion channel \mathcal{C} . As a result of this drift of ions within the electrolyte in the two reservoirs, eventually the measured potential drop across the reservoirs is zero and all the potential drop occurs across the ion channel. The applied external potential also results in an induced surface charge at the protein water dielectric boundary. The resulting potential within the channel is computed using Poisson's equation and stored in a 3-D lookup table. Indeed, in our BD simulation package, we combine the external applied potential with the fixed charges in protein (see discussion of PMF above) and then solve Poisson's equation as described above.

- 3) *Inter-ion Coulomb Potential*: In (5), $\Phi^{C,i}(\mathbf{X}_t)$ denotes the Coulomb interaction between ion i and all the other ions

$$\Phi^{C,i}(\mathbf{X}_t) = \frac{1}{4\pi\epsilon_0} \sum_{j=1, j \neq i}^{2N} \frac{q^{(j)}}{\epsilon_w \|\mathbf{x}_t^{(i)} - \mathbf{x}_t^{(j)}\|}. \quad (8)$$

- 4) *Ion-wall Interaction Potential*: The ion-wall potential Φ^{IW} , also called the $(\sigma/r)^9$ potential, ensures that the position of all ions $i = 1, \dots, 2N$ lie in \mathcal{R}^o . With $\mathbf{x}_t^{(i)} = (x_t^{(i)}, y_t^{(i)}, z_t^{(i)})'$, it is modeled as

$$\Phi^{IW}(\mathbf{x}_t^{(i)}) = \frac{F_0}{9} \frac{(r^{(i)} + r_w)^9}{\left[r_c + r_w - \left(\sqrt{x_t^{(i)2} + y_t^{(i)2}} \right) \right]^9} \quad (9)$$

where for positive ions $r^{(i)} = r^+$ (radius of positive ion) and for negative ions $r^{(i)} = r^-$ (radius of negative ion), $r_w = 1.4$ Å is the radius of atoms making up the wall, r_c denotes the radius of the ion channel, and $F_0 = 2 \times 10^{-10}$ N, which is estimated from the ST2 water model used in molecular dynamics [47]. This ion-wall potential results in short range forces that are only significant when the ion is close to the wall of the reservoirs \mathcal{R}_1 and \mathcal{R}_2 or anywhere in the ion channel \mathcal{C} (since the narrow segment of an ion channel can be comparable in radius to the ions).

- 5) *Short Range Potential*: Finally, at short ranges, the Coulomb interaction between two ions is modified by adding a potential $\Phi^{SR,i}(\mathbf{X}_t)$, which replicates the effects of the overlap of electron clouds. Thus

$$\Phi^{SR,i}(\mathbf{X}_t) = \frac{F_0}{9} \sum_{j=1, j \neq i}^{2N} \frac{(r^{(i)} + r^{(j)})}{\|\mathbf{x}_t^{(i)} - \mathbf{x}_t^{(j)}\|^9}. \quad (10)$$

Similar to the ion-wall potential, $\Phi^{SR,i}$ is significant only when ion i gets very close to another ion. It ensures that two opposite charge ions attracted by inter ion Coulomb forces (8) cannot collide and annihilate each other. Molecular dynamics simulations show that the hydration forces between two ions add further structure to the $1/\|\mathbf{x}_t^{(i)} - \mathbf{x}_t^{(j)}\|^9$ repulsive potential due to the overlap of electron clouds in the form of damped oscillations [48], [49]. Reference [45] incorporated the effect of the hydration forces in (10) in such a way that the maxima of the radial distribution functions for $\text{Na}^+ - \text{Na}^+$, $\text{Na}^+ - \text{Cl}^-$ and $\text{Cl}^- - \text{Cl}^-$ would correspond to the values obtained experimentally.

D. Probabilistic Interpretation of Brownian Dynamics

The aim of this subsection is to give a probabilistic characterization of the ion channel current. That is, Theorem 1 states that the mean ion channel current satisfies a boundary valued partial differential equation related to the Fokker-Planck equation. The BD simulation Algorithm 1 can then be viewed as a Monte Carlo simulation method for solving this partial differential equation. For simplicity of exposition, we assume in this subsection that as a result of the applied external potential, only positive ions traverse through the channel from \mathcal{R}_1 to \mathcal{R}_2 . In cationic channels, for example, only K^+ or Na^+ ions flow through to cause the channel current—so we do not need to consider the mean passage time of negative ions.

The dynamics of the BD simulation has an inherent two-time scale property. Typically, the time for an ion to enter and propagate through the ion channel is several orders of magnitude larger compared to the time it takes for an ions to move within a reservoir. That is the time constant for the particles in the reservoirs to attain steady state is much smaller than the time it takes for a particle to enter and propagate through the channel.

The following two-step probabilistic construction formalizes the probabilistic construction of BD.

Procedure 1: Probabilistic Construction of Brownian Dynamics Ion Permeation in Ion Channel:

Step 1: The $2N$ ions in the system are initialized in the reservoir and the ion channel \mathcal{C} is closed. The system evolves and attains stationarity.

Step 2: After stationarity is achieved, the ion channel is opened. The ions evolve according to (2) and (3). As soon as an ion from \mathcal{R}_1 crosses the ion channel \mathcal{C} and enters \mathcal{R}_2 , the experiment is stopped. Similarly, if an ion from \mathcal{R}_2 crosses \mathcal{C} and enters \mathcal{R}_1 , the experiment is stopped. Theorem 1 gives a partial differential equation for the mean time an ion in \mathcal{R}_1 takes to cross the ion channel and reach \mathcal{R}_2 . From this an expression for the mean ion channel current is constructed (13).

Remark: The above construction is a mathematical idealization. In the BD simulation Algorithm 1, the ion channel is kept open and ions that cross the channel are simply removed and replaced in their original reservoir. However, the above mathematical construction is a satisfactory approximation since due to the two time scale property, the time taken to attain this stationary distribution is much smaller than the time it takes for a single ion to cross the ion channel.

Let $\pi_t^{(\lambda)}(\mathbf{X}, \mathbf{V})$ denote the joint probability density function of the position and velocity of all the $2N$ ions at time $t \geq 0$. We explicitly denote the λ dependence of the probability density functions since they depend on the experimental condition $\lambda \in \Lambda$. The marginal probability density function $\pi_t^{(\lambda)}(\mathbf{X}) = p^{(\lambda)}(\mathbf{x}_t^{(1)}, \mathbf{x}_t^{(2)}, \dots, \mathbf{x}_t^{(2N)})$ of the positions of all $2N$ ions at time t is obtained as

$$\pi_t^{(\lambda)}(\mathbf{X}) = \int_{\mathbb{R}^{6N}} \pi_t^{(\lambda)}(\mathbf{X}, \mathbf{V}) d\mathbf{V}.$$

It is shown in [20] that $\pi_t^{(\lambda)}(\mathbf{X}, \mathbf{V})$ converges exponentially fast to its stationary (invariant) distribution $\pi_\infty^{(\lambda)}(\mathbf{X}, \mathbf{V})$. That is, the ions in the two reservoirs attain steady state exponentially fast.

We now proceed to Step 2 of the BD construction of Procedure 1. Assume that the BD system (2), (3) comprised $2N$ ions has attained stationarity with the ion channel \mathcal{C} closed according to Step 1. Now in Step 2 of Procedure 1, the ion channel is opened so that ions can diffuse into it.

Let $\tau_{\mathcal{R}_1, \mathcal{R}_2}^{(\lambda)}$ denote the mean minimum time for any of the $N/2$ positive ions in \mathcal{R}_1 to travel to \mathcal{R}_2 via the channel \mathcal{C}

$$\tau_{\mathcal{R}_1, \mathcal{R}_2}^{(\lambda)} = \mathbf{E}\{t_{\beta}\}. \quad (11)$$

To define the first passage time t_α , it is convenient to define

$$\begin{aligned} \zeta &= (\mathbf{X}, \mathbf{V}) \\ \mathcal{P}_2 &= \left\{ \zeta : \left\{ z^{(1)} \geq \beta \right\} \cup \left\{ z^{(2)} \geq \beta \right\} \cup \dots \cup \left\{ z^{(N/2)} \geq \beta \right\} \right\} \\ \mathcal{P}_1 &= \left\{ \zeta : \left\{ z^{(N/2+1)} \leq \alpha \right\} \cap \dots \cap \left\{ z^{(2N)} \leq \alpha \right\} \right\}. \end{aligned} \quad (12)$$

Here, $z^{(i)}$ denotes the z -axis spatial coordinate of the i th ion. Then, $t_\beta = \inf\{t : \zeta_t \in \mathcal{P}_2 | \zeta_0 \in \mathcal{P}_1\}$.

In terms of the mean first passage time $\tau_{\mathcal{R}_1, \mathcal{R}_2}^{(\lambda)}$ defined in (11), the mean current flowing from \mathcal{R}_1 via the ion channel \mathcal{C} into \mathcal{R}_2 is defined as

$$I^{(\lambda)}(\theta) = \frac{q^+}{\tau_{\mathcal{R}_1, \mathcal{R}_2}^{(\lambda)}}. \quad (13)$$

The following result adapted from [50, p. 306] shows the mean passage time $\tau_{\mathcal{R}_1, \mathcal{R}_2}^{(\lambda)}$ and satisfies a boundary valued partial differential equation (see also [51]). In particular, the expressions for the mean passage time below, together with (13), give a complete characterization of the ion channel current.

Theorem 1: Consider the two step BD probabilistic construction in Procedure 1. Then, the mean first passage time $\tau_{\mathcal{R}_1, \mathcal{R}_2}^{(\lambda)}$ [defined in (13)] for ions to diffuse through the ion channel are obtained as

$$\tau_{\mathcal{R}_1, \mathcal{R}_2}^{(\lambda)} = \int_{\mathcal{P}_1} \tau_{\mathcal{R}_1, \mathcal{R}_2}^{(\lambda)}(\zeta) \pi_\infty^{(\lambda)}(\zeta) d\zeta. \quad (14)$$

Here, $\tau_{\mathcal{R}_1, \mathcal{R}_2}^{(\lambda)}(\zeta)$ satisfies the following boundary value partial differential equations:

$$\mathcal{L}\left(\tau_{\mathcal{R}_1, \mathcal{R}_2}^{(\lambda)}(\zeta)\right) = -1 \quad \zeta \notin \mathcal{P}_2, \quad \tau_{\mathcal{R}_1, \mathcal{R}_2}^{(\lambda)}(\zeta) = 0 \quad \zeta \in \mathcal{P}_2 \quad (15)$$

where for any test function $\phi(\cdot)$, \mathcal{L} denotes the backward elliptic operator (infinitesimal generator)

$$\mathcal{L}(\phi) = \frac{1}{2} \text{Tr} \left[\Sigma \nabla_\zeta^2 \phi(\zeta) \right] + (\mathbf{f}_{\theta, \lambda}(\zeta) + \mathbf{A}\zeta)' \nabla_\zeta \phi(\zeta). \quad (16)$$

Remark: The previous partial differential equation cannot be solved in closed form—so the BD simulation Algorithm 1 can be viewed as a randomized numerical method for solving this partial differential equation. We show in Section IV that the BD simulation algorithm can be successfully used to predict the function of several important types of ion channels.

E. Discussion

In the above BD formulation the forces acting on charged particles were calculated by solving the macroscopic (bulk) Poisson's equation (7). In bulk water,

molecules polarize to shield electrostatic interactions by a factor of approximately 1/80. However, given the likely preferential alignment of water in narrow pores and regions of high charge, this shielding is likely to be far less effective in an ion channel. Thus, one should use a lower value of the dielectric constant ϵ_{water} for the water in the channel when solving Poisson's equation (7). But exactly what value of the dielectric constant should be used is unknown. Determining the appropriate values using molecular dynamics simulations or otherwise would be a useful project.

Assigning the appropriate value of the dielectric constant of protein $\epsilon_{\text{protein}}$ in (7) is also nontrivial. Unlike water and lipids, which form homogeneous media, proteins are quite heterogeneous, exhibiting large variations in polarizability depending on whether we are dealing with the interior or exterior of a protein [52]. There are several molecular dynamics studies of the dielectric constant of protein [53]–[55]. The dielectric constant for the whole protein varies between 10 and 40, but when only the interior region of the protein consisting of the backbone and uncharged residues is considered, the value drops to 2 or 4. The effects of changing the dielectric constant of protein from 3.5 and 5 were examined by [56] using the KcsA potassium channel. They showed that the precise value adopted in solving Poisson's equation has negligible effects on the macroscopic properties derived from BD simulations.

The validity of treating the channel protein as a static structure in BD also deserves further investigation. It should be noted that thermal fluctuations of proteins occur in the time-scale of femto seconds, whereas a conduction event across a typical ion channel takes place once in 100 ns—approximately six to seven orders of magnitude slower time scale. Thus, it is likely that rapid thermal fluctuations of the atoms forming the channel are not important for channel selectivity and conduction. This can be shown using stochastic averaging methods in nonlinear dynamical systems (e.g., [27]). Alterations in the average positions of the protein atoms caused by the presence of permeating ions may play a role, and their effects should be examined both experimentally and by using molecular dynamics simulations. If found to be important, some of the motions of the protein, such as the bending of carbonyl groups, can readily be incorporated in BD modeling of ion channels. Finally, size-dependent selectivity among ions with the same valence cannot be easily understood within the BD framework, and one has to appeal to molecular dynamics or semi-microscopic Monte Carlo simulations [57].

IV. APPLICATION OF BD IN ION CHANNELS

The BD modeling and simulation methodology described in Section III has been fruitfully utilized in

satisfactorily capturing the macroscopic behavior of several specific ion channels. In this section, we summarize the performance of BD for three important classes of biological ion channels: the KcsA potassium channel, the L-type calcium channel, and the anionic CLC Cl^- channel.

A. Potassium Channels

KcsA K^+ Channel: A number of computational studies using molecular dynamics [24], [58]–[63] and semi-microscopic approaches [44], [64], [65] have been carried out on the KcsA potassium channel, the first biological channel whose crystal structure has been determined. These studies have elucidated, among others, the basis of ion selectivity, the mechanisms underlying the permeation of ions across the channel, and the conformational changes that occur in the KcsA protein when the channel opens. Detailed summaries of the main findings are given in several recent review articles [66], [67]. Here, we outline the main results obtained from BD simulations on the KcsA channel.

The KcsA structure determined from X-ray diffraction consists of 396 amino acid residues, or 3504 atoms excluding polar hydrogens. The channel is constructed from four subunits of peptide chains, each subunit consisting of an outer helix, inner helix, pore helix, and a threonine–valine–glycine–tyrosine–glycine (TVGYG) amino acid sequence that forms the selectivity filter. The protein atoms form a central pore between these subunits. The shape of the ion-conducting pathway across the KcsA protein is illustrated in Fig. 2, where two of the four subunits of the full experimentally determined protein are shown. Water molecules residing inside and just outside of the pore shown as gold balls in Fig. 2(a). An outline of the pore reveals that the channel is composed of three segments—a long intracellular region of length 20 Å lined with hydrophobic amino acids extending towards the intracellular space (left-hand side), a wide water-filled chamber of length 10 Å, and a narrow selectivity filter of length 12 Å, extending towards the extracellular space. The selectivity filter is the most important element in this structure as it can distinguish K^+ ions from those of Na^+ on the basis of their sizes (the crystal radius of K^+ is 1.33 Å and that of Na^+ is 0.95 Å). The aspartate–arginine pair near the extracellular entrance (right-hand side) and the glutamate–arginine pair near the intracellular entrance (left-hand side) are indicated in red and silver. BD simulations show that there are three regions in the selectivity filter and cavity where K^+ ions dwell preferentially. There is also another prominent binding site near the intracellular entrance of the channel. The preferred positions where ions dwell preferentially are in close agreement with the positions observed in Rb^+ X-ray diffraction maps [7].

To illustrate the permeation mechanism across the potassium channel, we bisect the channel such that ions in

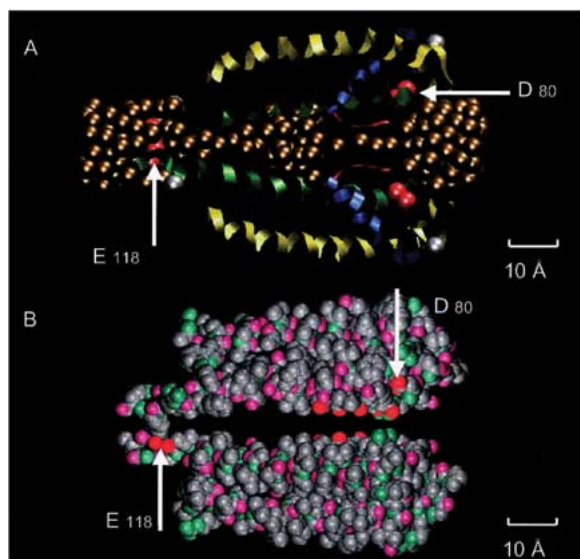


Fig. 2. Model potassium channel. (a) Two of four subunits of full experimentally determined *KcsA* potassium channel and positions of water molecules (gold) inside pore are illustrated. Here, helices of channel protein are represented in ribbon form. Aspartate-arginine pairs near the extracellular entrance of the channel (right-hand side) and glutamate-arginine pair near intracellular entrance of the channel are indicated in red and silver. (b) Outline of the water-protein boundary of a channel is shown. For clarity, top and bottom subunits are removed.

the chamber and filter found during BD simulations are consigned to the right side, and the rest to the left side. The most common situation in the conducting state of the channel has one ion in the left half, and two ions in the right half. We refer to this configuration as the [1, 2] state. A typical conduction event consists of the following transitions: $[1, 2] \rightarrow [0, 3] \rightarrow [0, 2] \rightarrow [1, 2]$. In other words, the ion waiting near the intracellular mouth overcomes a small energy barrier in the intracellular pore to enter the chamber region. Because this system is unstable in the presence of an applied potential, the right-most ion is ejected from the channel. Another ion enters the intracellular mouth, leaving the system in its original configuration. The precise sequence of events taking place for conduction of ions depends on their concentration, applied potential, and the ionization state of charged residues at the intracellular gate, and many other states can be involved in the conduction process depending on the values of these variables. Simulations also reveal that permeation across the filter is much faster than in other parts of the channel. That is, once a third ion reaches the oval cavity, the outermost ion in the selectivity filter is expelled almost instantaneously. Thus, although the filter plays a crucial role in selecting the K^+ ions, its role in influencing their conductance properties is minimal.

Fig. 3(a) and (b) shows the current-voltage and current-concentration curves obtained from BD simulations [56]. The results of BD simulations are in broad agreement with those determined experimentally [68]–[70]. With the radius of the intracellular gate expanded to 4 Å, we obtain the conductances at +150 mV and –150 mV of, respectively, 147 ± 7 and 96 ± 4 pS. The relationship is linear when the applied potential is in the physiological range but deviates from Ohm's law at a higher applied potential, especially at high positive potentials. The current saturates with increasing ionic concentrations, as shown in Fig. 3(b). Experimentally, the current $I^{(\lambda)}$ across many channels first increases with an increasing potassium ionic concentration $\lambda = [K]$ and then saturates. (As usual, λ denotes the experimental condition, i.e., the potassium concentration denoted $[K]$ in this case.)

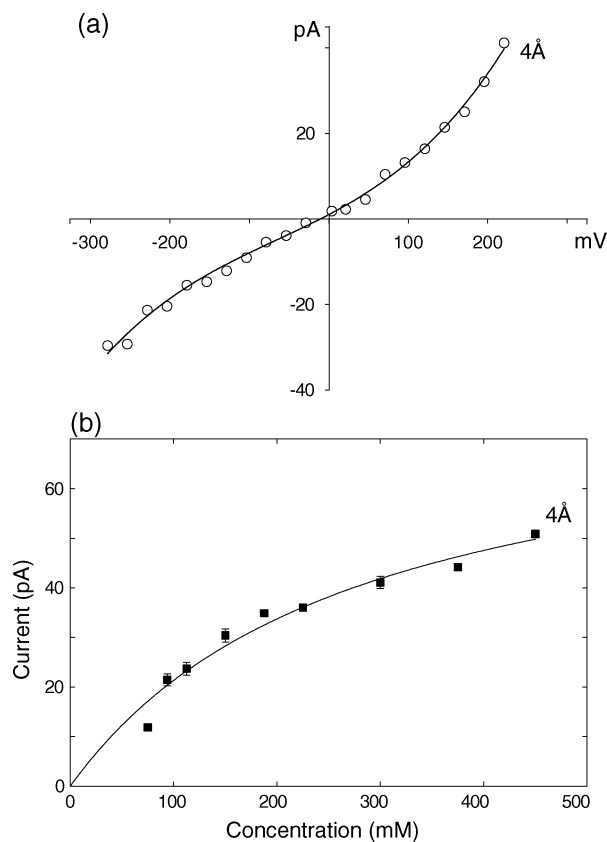


Fig. 3. Current-voltage-concentration profile deduced from BD simulations. (a) Current passing through channel with a symmetric solution of 300 mM KCl in both reservoirs is plotted against applied potential. Relationship is linear when applied potential is less than ± 150 mV but deviates systematically from Ohm's law with a further increase in the membrane potential. (b) The current-concentration relationship is obtained with symmetrical solutions of varying concentrations of KCl in the reservoirs, with applied potential of 221 mV. Data points are fitted by a solid line using (17). Half-saturation value $[K_s]$ deduced from the fitted curve is 277 ± 54 mM.

This behavior leads to a current-concentration relationship of the Michaelis–Menten form

$$I^{(\lambda)} = \frac{I_{\max}}{1 + [K_s]/[K]} \quad (17)$$

Here, $[K_s]$ denotes the half-saturation point of the ion channel. According to (17), the current $I^{(\lambda)}$ approaches the saturation current I_{\max} when $[K] \gg [K_s]$. Theoretically, the conductance-concentration curve is expected to saturate if the transport of ions across the channel is determined by two independent processes: the time it takes for an ion to enter the channel mouth depends on the concentration, while the time it takes for the ion to reach the oval chamber is independent of the concentration but depends solely on the applied potential.

Modeling Other Potassium Channels: There are many different types of potassium channels, which differ widely in their conductances and gating characteristics while having a similar primary structure. Conductance levels of various types of potassium channels range from 4 to 270 pS (1 pS equals 0.1 pA of current across the channel with the driving force of 100 mV). Despite this diversity, they all share the common feature of being highly selective to potassium ions and display broadly similar selectivity sequences for monovalent cations. Also, the amino acid sequence of the peptide chains lining the selectivity filter of all potassium channels is known to be highly conserved. Thus, it is likely that the diversity of potassium channels results from structural changes on the protein architecture near the intracellular segment of the pore, which have very different sequences.

Using BD simulations, [71] explored whether the widely differing properties of potassium channels found in nature can be understood by small modifications of the channel geometry. Using the experimentally determined potassium channel structure as a template, as shown in Fig. 4(a), they systematically changed the radius of the intracellular pore entrance, leaving the dimensions of the selectivity filter and cavity unaltered. By examining the energy profiles and the probabilities of ion occupancies in various segments of the channel, they deduce the rate-limiting step for conduction in the potassium channels. Ion distributions revealed that the selectivity filter is occupied by two K^+ ions most of the time. Potential energy profiles encountered by a third ion traversing along the central axis of the channel when there are two ions in or near the selectivity filter are shown for the channels with radii 2 Å [solid line in Fig. 4(b)], 3 Å (long-dashed line), and 4 Å (dashed line). Ions need to climb over the energy barrier, whose height is denoted as ΔU , to move across the channel. This barrier is the rate-limiting step in the permeation process: as its height increases with a

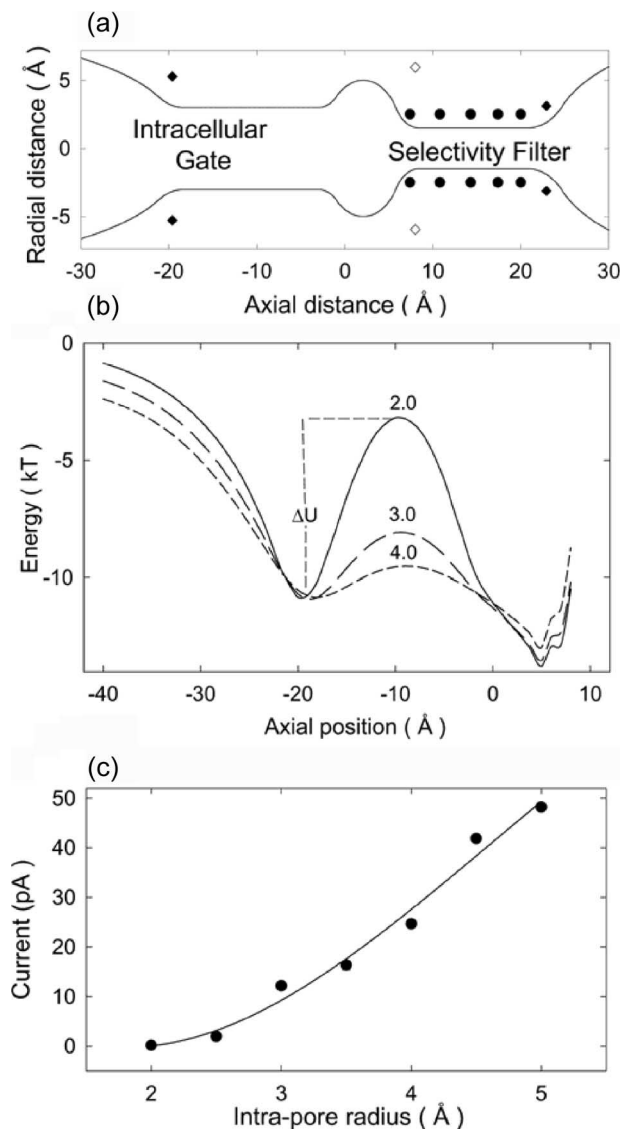


Fig. 4. Models of potassium channels. (a) Shape of KcsA channel is modified such that minimal radius of the wider segment is 3 Å. Solid line shows outline of a simplified model channel. Three-dimensional channel is obtained by rotating curves about the central axis by 180°. The 10 of 20 oxygen atoms lining the pore are shown in filled circles. Locations of aspartate and glutamate residues guarding extracellular and intracellular gates are shown in filled diamonds. Radii of intracellular gate were varied from 2 to 5 Å. (b) Potential energy profiles encountered by an ion traversing along central axis of channel, when there are two other ions in or near the selectivity filter, are shown for the channels with radii 2, 3, and 4 Å. Ions need to climb over energy barrier, whose height is denoted as ΔU , to move across channel. (c) Outward current is plotted against radius of intracellular aspect of channel entrance.

decreasing intra-pore radius, the channel conductance drops exponentially. As the intra-pore radius is increased from 2 to 5 Å, the channel conductance changes from 0.7 to 197 pS (0.17 to 48 pA). In Fig. 4(c), the simulated current across the model ion channel determined from BD

is plotted against the radius of the intra-pore gate. Thus, the diversity of potassium channels seen in nature is achieved by slightly altering the geometry of the intracellular aspect of the channel macromolecule.

B. CLC Chloride Channels

BD simulations were similarly applied to elucidate the dynamics of ion permeation across CLC-type channels [72]. The prototype channel, known as CLC-0, first discovered and characterized by [73], is found in *Torpedo electroplax*. Since then, nine different human CLC genes and four plant and bacterial CLC genes have been identified. The CLC family of Cl^- channels is present in virtually all tissues—in muscle, heart, brain, kidney and liver—and is widely expressed in most mammalian cells. By allowing Cl^- ions to cross the membrane, CLC channels perform diverse physiological roles, such as control of cellular excitability, cell volume regulation, and regulation of intracellular pH [74]. Dutzler *et al.* [8], [9] determined the X-ray structure of a transmembrane CLC protein in bacteria that has subsequently been shown to be a transporter, not an ion channel [75]. Nevertheless, many amino acid sequences of the bacterial CLC protein are conserved in their eukaryotic CLC relatives, which are selectively permeable to Cl^- ions.

We refer the reader to [72] for details on the homology model construction of a CLC-0 channel atomic model. As illustrated in Fig. 5(a), the ionic pathway of CLC-0 takes a tortuous course through the protein, unlike that of the potassium channel, which is straight and perpendicular to the membrane surface. The channel is quite narrow, having a minimum radius of 2.5 Å near the center, but opens up quite rapidly at each end. The distance from one end of the pore to the other is 55 Å and it is lined with many charged and polar amino acid residues. Incorporating this homology model into BD, they determined the current–voltage–concentration profile of CLC-0. A current–voltage relationship obtained with symmetrical solutions of 150 mM in both reservoirs is shown in Fig. 5(b). The relationship is linear, with a conductance of 11.3 ± 0.5 pS that agrees well with experimental measurements reported by [73] (superimposed open circles). The slope conductance determined from the experimental data is 9.4 ± 0.1 pS. The current–concentration relationship obtained from the homology model using BD (filled circles) is also in accord with the experimental observations as shown in open circles in Fig. 5(c). The lines fitted through the data points are calculated from the Michaelis–Menten equation (17). There is a good agreement between the simulated data and experimental measurements for CLC-0.

BD simulations also reveal the steps involved in permeation of Cl^- ions across the CLC channel. The pore is normally occupied by two Cl^- ions. When a third ion enters the pore from the intracellular space [left-hand side in the inset of Fig. 5(a)], the stable equilibrium is

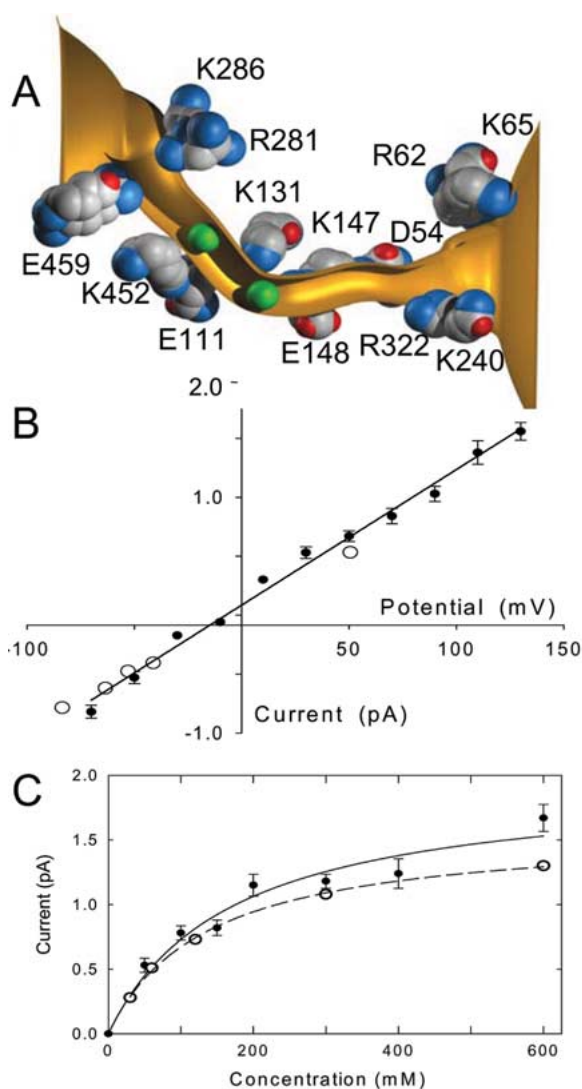


Fig. 5. BD simulations of CLC-0. (a) Locations of charged residues lining the pore of CLC-0 are illustrated. The locations of arginine (R) and lysine (K) (positively charged) residues and aspartate (D) and glutamate (E) (negatively charged) residues lining the ion-conducting path are shown. Intracellular aspect of channel is on left-hand side. (b) Current measured at various applied potentials (filled circles) is obtained with symmetrical solutions of 150 mM in both reservoirs. Superimposed on the simulated data are experimental measurements obtained in [73], shown in open circles. (c) Outward currents (filled circles) are obtained with symmetrical solutions of varying concentrations of NaCl in reservoirs under an applied potential of -80 mV. Data points are fitted by solid line using the Michaelis–Menten equation. Unpublished experimental measurements obtained by Dr. T.-Y. Chen (personal communication) are shown in open circles.

disrupted, and the outermost Cl^- ion is expelled to the extracellular space.

C. Calcium Channels

Calcium channels are necessary for several important physiological functions, such as the contraction of cardiac

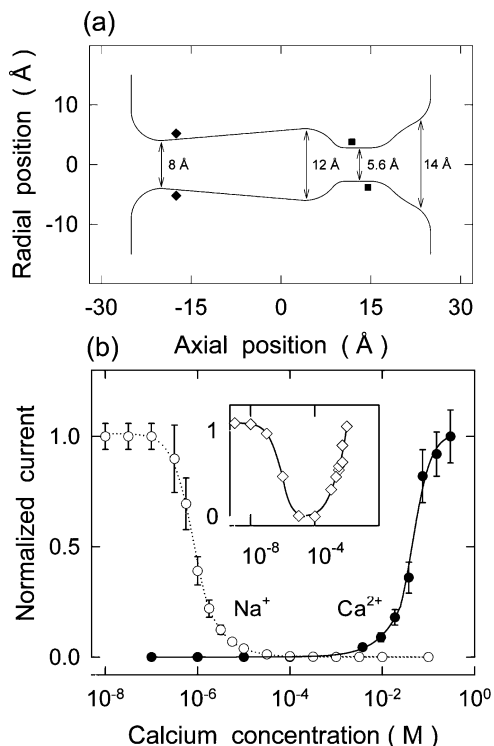


Fig. 6. Minimal model of L-type calcium channel and anomalous mole fraction curve deduced from BD simulations. (a) Three-dimensional channel model is generated by rotating curves about central axis by 180° . Positions of two of four glutamate groups are shown by the filled squares, and inner end of two of four mouth dipoles by the filled diamonds. Intracellular side of the channel is on left-hand side. (b) Ca^{2+} (filled circles) and Na^+ (open circles) currents across channel determined with different symmetrical calcium concentrations in reservoirs from BD simulations are plotted. Sodium concentration is held fixed at 150 mM in both reservoirs, and current was measured with an applied potential of -200 mV. Experimental measurements obtained by [76] are shown in inset for comparison.

and skeletal muscles and communication between cells. To perform these roles, they must exhibit remarkable selectivity while conducting millions of ions into the cell every second. Biophysical studies on calcium channels reveal many complex properties. Sodium ions can move across calcium channels in the absence of calcium ions, but as soon as a small concentration of calcium ions is introduced, conduction of sodium ions is completely blocked. Channels become exquisitely selective, selecting calcium over sodium at a ratio of 1000 : 1. To date, the crystal structure of any type of calcium channels has not been determined. Reference [45] constructed a minimal model of the L-type calcium channel, making use of many of their known experimental properties. A 3-D model was generated by rotating the curves shown in Fig. 6 by 180° . The important features of the model are a wide extracellular entrance chamber, a narrow selectivity filter ($r = 2.8$ Å) with four point charges, representing gluta-

mate residues, placed in a helical pattern (two of which are shown in filled squares), and a long chamber region that tapers toward the intracellular entrance (left-hand side). Four mouth dipoles (two of which are shown in filled diamonds) were placed at the intracellular entrance to overcome the image forces. These dipoles are also represented as point charges. Thus, the channel is constructed as a homogeneous, featureless low dielectric material with the dielectric constant of 2, through which an ion-conducting pathway is bored.

Despite its simplicity, the model, when incorporated into a BD simulation assembly, reproduced many of the remarkable biophysical findings. The deep energy well created by four point charges along the selectivity filter attracted two sodium ions when the reservoirs contained 150 mM NaCl and one calcium ion when NaCl was replaced with CaCl_2 . A third Na^+ ion entering the selectivity filter from the intracellular reservoir disrupts the stable equilibrium established by the two resident Na^+ ions and expels the outermost ion to the extracellular reservoir. Similarly, a second Ca^{2+} ion entering the selectivity filter expels the resident Ca^{2+} ion. Thus, the conduction across the channel for both monovalent and divalent ions is a multi-ion process. The current-voltage-concentration profiles for Na^+ and Ca^{2+} ions obtained from BD simulations broadly mirrored the experimental findings.

Experimental studies of mixtures of Ca^{2+} and Na^+ ions in calcium channels have shown a remarkable behavior. As the relative concentration of Ca^{2+} to Na^+ is decreased, the conductance of the channel first decreases to a minimum and then increases again to a maximum where there is no Ca^{2+} present [76]. This so-called “anomalous mole fraction effect” has been a major subject of attention in calcium literature. Using the minimal model illustrated in Fig. 6(a), [45] investigated this behavior using electrostatic calculations as well as in BD simulations. They showed that when a Ca^{2+} entered the selectivity filter of the channel, it would bind there tightly so that a Na^+ ion could not displace it via Coulomb repulsion. Thus, sodium conduction, once a Ca^{2+} entered the channel, would cease. On the other hand, another Ca^{2+} ion entering the selectivity filter, owing to a greater Coulomb force it could exert on the resident ion, was able to displace it, allowing calcium conduction to take place. In BD simulations, they fixed the Na^+ concentration at 150 mM and measured the channel current at different Ca^{2+} concentrations. The values of the calcium and sodium current at different calcium concentrations, normalized by the maximum value of each, are shown by the filled and open circles in Fig. 6. As the calcium concentration decreased, the Ca^{2+} current also decreased. With further reduction in calcium concentration, it would take longer for a calcium ion to enter and block the channel, thus allowing more Na^+ ions to pass through the channel. The experimental measurements of [76] are shown in the inset for comparison. The figure shows how the complex behavior of the calcium channel

can arise from simple electrostatic interactions between ions, the channel boundary, and the charges therein.

V. ACBD FOR ION CHANNELS: FORMULATION

In Section IV, we illustrated how BD can be used as a valid theory for explaining permeation in several types of ion channels. What this means is that the simulated BD current $\hat{I}^{(\lambda)}$ under various simulated experimental conditions $\lambda \in \Lambda$ matches the actual experimental observed current $I^{(\lambda)}$. (Recall that Λ denotes the set of experimental conditions.) Thus, for such channels BD provides a valid theory for relating atomic structure of the ion channel to macroscopic function. However, as discussed in Section II and Section III-E, BD does not explain permeation for particularly narrow ion channels such as gramicidin or within the selectivity filter of a sodium channel.

The method of ACBD we propose in this section is designed to circumvent the limitations posed by the traditional BD simulation approach. In ACBD, we solve an inverse estimation problem. That is, given the 3-D atomic model of an ion channel, we directly estimate the PMF of a gramicidin channel or the shape of a sodium channel that best replicates experimental observations $I^{(\lambda)}$ for a variety of experimental conditions $\lambda \in \Lambda$. Thus, ACBD estimates the *effective PMF* or *effective shape* that minimizes the mean square error between the BD simulated current and the actual observed experimental current. The advantage of directly estimating the effective PMF or shape is that it completely removes the requirement of solving Poisson's equation (7). Thus, the problem of assigning the effective dielectric constants of the pore and of the protein is avoided. Second, no assumption about the ionization state of some of the residues lining the pore has to be made.

A. ACBD as Stochastic Optimization Problem

Let θ denote a finite-dimensional parameter that characterizes either the PMF of a gramicidin channel or the shape of a sodium channel. From experimental data, an accurate estimate of the current-voltage-concentration profiles of an ion channel can be obtained. These curves depict the actual current $I^{(\lambda)}$ flowing through an ion channel for various external applied potentials $\lambda \in \Lambda$ and ionic concentrations. Suppose that the BD simulation Algorithm 1 is run in batches indexed by batch number $n = 1, 2, \dots$. In each batch n , the PMF parameter θ_n is selected (as described in the following), the experimental condition (applied potential and concentration) $\lambda \in \Lambda$ is applied, and the BD Algorithm 1 is run over L iterations, then the estimated current $\hat{I}_n^{(\lambda)}(\theta)$ is computed using (4). Define the square error loss function as

$$C(\theta) = \mathbf{E}\{C_n(\theta)\}, \quad C_n(\theta) = \sum_{\lambda \in \Lambda} \left(\hat{I}_n^{(\lambda)}(\theta) - I^{(\lambda)} \right)^2. \quad (18)$$

The total loss function $C(\theta)$ is obtained by adding the square error over all the applied fields $\lambda \in \Lambda$ on the current-voltage or current-concentration curve. Our aim is to compute the optimal parameter $\theta^* \in \Theta$ where Θ denotes the set of feasible parameters and

$$\theta^* = \arg \min_{\theta \in \Theta} C(\theta). \quad (19)$$

Note that (18) and (19) constitute a stochastic optimization problem, since we do not have a closed form expression for $C(\theta)$ —instead only noisy estimates $C_n(\theta)$ of the cost function are available in terms of the BD simulated current $\hat{I}_n^{(\lambda)}(\theta)$ for different experimental conditions $\lambda \in \Lambda$.

Depending on whether the parameter space Θ is a compact subset of the reals or a finite set, (19) can be formulated as a *continuous-valued* or *discrete-valued* stochastic optimization problem. For example, we consider the continuous case where Θ is a compact subset of the reals representing the means and variances of Gaussian basis functions used to fit the PMF U_θ for gramicidin channels. Another example, considered as follows, is the discrete case where $\Theta = (1, 2, \dots, S)$ denotes S feasible shapes of the sodium channel.

B. Example 1: Estimating PMF of Gramicidin Channels

Gramicidin is an antibiotic produced by *Bacillus brevis* [77, p. 130]. In this section, we formulate the PMF estimation problem for a gramicidin channel as a stochastic optimization problem of the form (18).

Why PMF estimation of Gramicidin? Since the structure of gramicidin channels are simple and well known, they are a useful benchmark for computational models that seek to explain ion permeation. Also, since the radius of gramicidin channels is much smaller than other biological ion channels, it has been recently been shown that the PMF U in (5) obtained by solving the macroscopic Poisson's equation (7) does not yield accurate results that fit experimental data [23]. Moreover, the PMF calculated along the gramicidin channel axis using molecular dynamics (MD) yields unrealistically large central barriers for a permeating ion, e.g., [25], [78]. When such a PMF is incorporated into nonequilibrium permeation models, it fails to replicate the experimental measurements.

Let us parameterize the PMF U in (5) by U_θ , where $\theta \in \Theta$ denotes a finite-dimensional parameter vector. We will consider the case where Θ is a compact subset of the reals and also the case where Θ is a finite set. For the gramicidin channel, we will represent $U_\theta(\cdot)$ by a Gaussian mixture with parameter vector θ and then present a stochastic algorithm to estimate θ . Any basis function approximation of the gramicidin PMF $U_\theta(\mathbf{x})$ needs to

capture the following important properties of the gramicidin channel.

- 1) The PMF $U_\theta(\mathbf{x})$ (where $\mathbf{x} = (0, 0, z)$) experienced by the ion within the gramicidin channel is symmetric with respect to z , i.e., $U_\theta(\mathbf{x}) = U_\theta(0, 0, z) = U_\theta(0, 0, -z)$ for all $\mathbf{x} \in \mathcal{C}$.
- 2) For $z < -20 \text{ \AA}$ or $z > 20 \text{ \AA}$, $U_\theta(z)$ should be close to zero since the PMF only acts on ions in or near the ion channel.

By using physiological data of the gramicidin channel, we find that the following scaled Gaussian mixture comprised of a linear combination of three Gaussian density functions gives an excellent fit:

$$U_\theta([0, 0, z]) = m \exp\left(-\frac{1}{2} \frac{(z - W)^2}{\sigma^2}\right) + m \exp\left(-\frac{1}{2} \frac{(z + W)^2}{\sigma^2}\right) + m_0 \exp\left(-\frac{1}{2} \frac{z^2}{\sigma_0^2}\right) \quad (20)$$

$$\theta = (W, \sigma^2, m, \sigma_0^2, m_0)'. \quad (21)$$

It is obvious that the parameterization satisfies the symmetry property 1. Also, for a suitable choice of the parameter vector θ in (21), property 2 holds. The structure of the gramicidin channel implies that the parameters θ defined in (21) need to be constrained to the set Θ defined as follows:

$$\Theta = \{W \in [0, 30 \text{ \AA}], \quad \sigma^2, \sigma_0^2 \in [0, \sigma_{\max}^2], \quad m, m_0 \in [0, M]\} \quad (22)$$

where M and σ_{\max} are positive bounded constants.

C. Example 2: Estimating Shape of Sodium Channel

Here, we formulate the estimation of the shape of a sodium channel as a discrete stochastic optimization problem of the form (18).

To motivate the shape estimation problem for sodium channels, let us first describe several of its salient features. A sodium channel has several unique properties that need to be captured by a simulation model. First, the sodium channel allows over 10^6 ions through the channel every second and yet is able to distinguish between sodium and other ions. Second, it has a high affinity for monovalent ions, is rapidly blocked by divalent ions, and allows no anions through. Third, the channel exhibits a symmetric, linear current-voltage curve when there are symmetric concentrations of NaCl in the intra-cellular and extra-cellular regions, and the current rapidly saturates with increasing concentrations. Finally, the channel is completely blocked when divalent ions are present in the

external solution but only marginally reduced in presence of intracellular divalent ions.

A sodium channel is comprised of four functional components: *external vestibule*, *selectivity filter*, *internal pore*, and *internal entrance region*. The family of sodium channels is believed to be structurally similar to the family of potassium ion channels. Thus, we have based the feasible shapes of the sodium channel on the KcsA potassium channel, the structure of which was recently crystallized by Doyle *et al.* [7]. We have shortened the selectivity filter and added an external vestibule to the existing potassium channel shape. Here, we describe in detail how by varying the dimensions of the above structural components there is a finite number of distinct possibilities for the shape. The candidate channels are depicted in Fig. 7 and the various parameters of these candidate channels are given in Table 1.

- 1) *Outer Vestibule*: The outer regions making up the sodium channel protein are believed to be composed of the P loops of the protein that form a conical outer vestibule [79], [80].
- 2) *Selectivity filter*: Similar to the KcsA, we include a short selectivity filter followed by an internal pore region. All channel models contain a selectivity filter with a radius of $r = 2.2 \text{ \AA}$ derived from permeant cation studies in [81]. As the length of the filter is unknown, we vary this parameter to fit the current. We use only the two charged rings suspected to lie in the selectivity filter and known from mutation studies to have a large effect on selectivity and conductance of the sodium channel [82]–[84]. The two charged rings are placed around the filter region as point charges, 1 \AA behind the protein boundary, at a distance of $z = 14 \text{ \AA}$ and $z = 18.5 \text{ \AA}$ from the central axis of the channel. The inner ring contains a positively charged lysine and a negatively charged glutamate and aspartate amino acid group, and the outer ring contains two negatively charged glutamates and two negatively charged aspartates. The positive lysine in the inner ring is fully charged, but we believe that more than one negative residue is likely to be protonated. For the position and charged states of these residues we have used the data of [85]. They find that two residues must be protonated at any given time to reproduce the experimental data. The inner ring has a total charge of $-1.0 \times 10^{-19} \text{ C}$ on average, where the lysine has the charge of one proton, and the negative residues in the inner ring a charge of $-1.3 \times 10^{-19} \text{ C}$ each. The outer ring contains a total charge of $3.8 \times 10^{-19} \text{ C}$ where the total charge is shared equally among all four negative residues, giving each residue a charge of $0.95 \times 10^{-19} \text{ C}$. We distribute equal charges among all residues in a ring because the exact charge state of any residue at a given time is

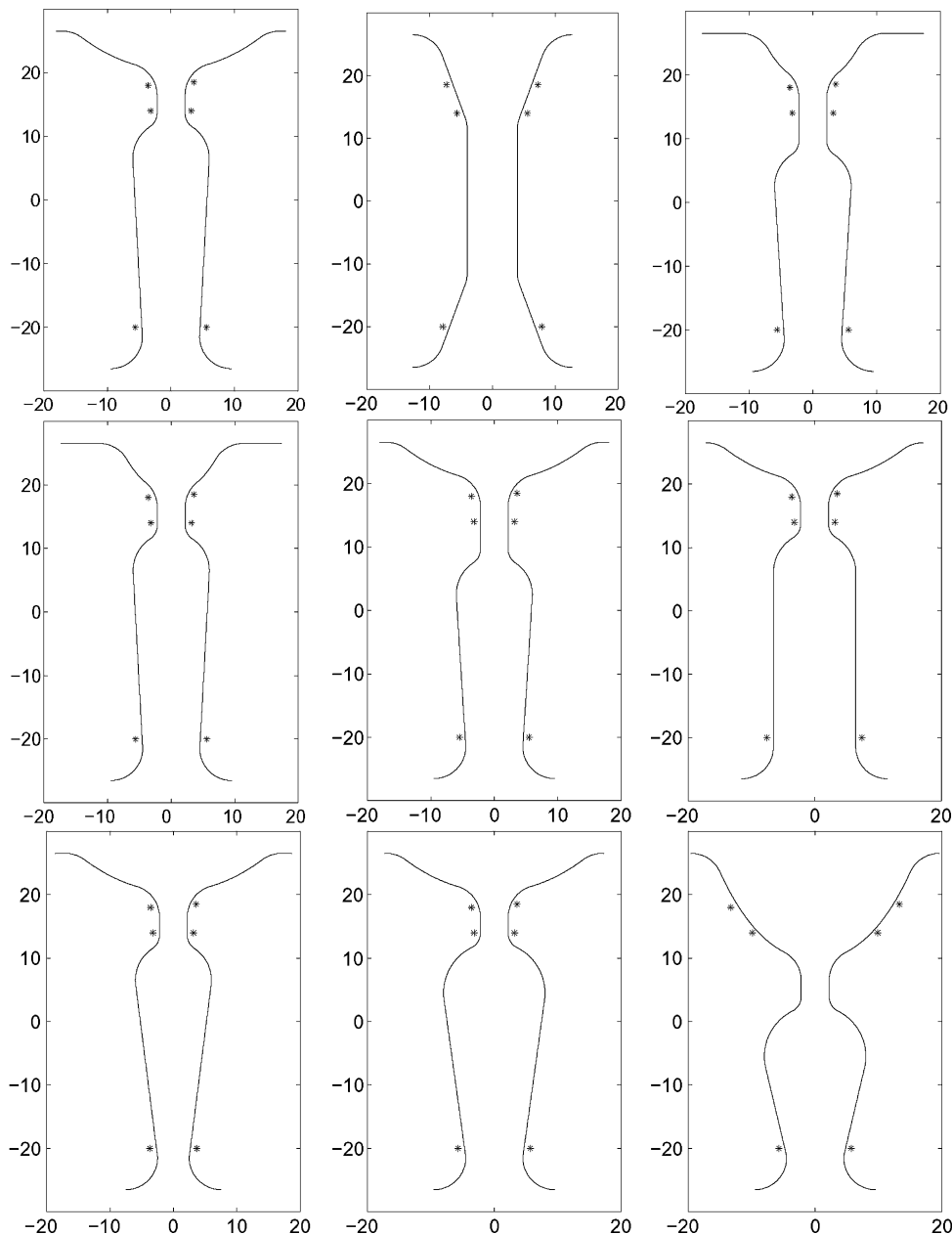


Fig. 7. *Nine candidate channel shapes for sodium channels considered in this paper. Six dots in each figure denote point charges in protein lining inner wall of ion channel—all units are in angstrom units Å (1 Å = 10⁻¹⁰ m). Upper four dots represent point charge approximations of two charged rings in selectivity filter, and bottom two dots in internal entrance of ion channel represent dipole charges that mimic intracellular helix dipoles of sodium channel protein.*

difficult to calculate; only the average behavior of the charged residue can be estimated.

- 3) *Inner pore:* Followed by the selectivity filter is an inner vestibule region. This is again adopted from the KcsA structure. The diameter and length of this region is unknown and has been varied in the shape estimation of the channel.
- 4) *Internal entrance:* The internal entrance leads into the inside of the cell. This region contains the

carboxyl end of the protein making up the sodium channel. For this reason, we include a set of dipole charges at $z = -20$ Å, mimicking the intracellular helix dipoles of the channel protein. The magnitude of charge on the helix dipoles is 0.6×10^{-19} C. The negative end is nearer to the channel entrance; the positive ends are buried deep inside the protein, and its effect is negligible.

Table 1 Nine Candidates for Channel Shapes of Sodium Channel

Shape	Radius			Height		
	Outer vestibule	Cavity	Inner pore	Outer vestibule	Selectivity filter	Inner pore
1	14	6	4.5	10	4	28
2	8	0	0	15	0	0
3	7	6	4.5	10	8	28
4	7	6	4.5	10	4	28
5	14	6	4.5	10	8	24
6	14	6.5	6.5	10	4	27.5
7	14	6	2.5	10	4	28
8	14	8	4.5	10	4	26
9	15	8	4.5	20	4	16

The channel model is generated by creating an initial outline of the channel pore and then rotating it by 180° to create a 3-D shape. Cylindrical symmetry is assumed with the channel centered around $z = 0$ Å and extending out to $z = \pm 27$. An extracellular and intracellular reservoir, R_1 and R_2 , is attached to either ends of the channel. The channel model has been varied systematically, all shapes used are given in Fig. 7 and Table 1. On the above-stated basic outline (of outer vestibule, selectivity filter, inner pore, and internal entrance), we have varied the dimensions of the channel to obtain currents through each individual channel. The parameters that were varied are stated in Table 1. We have varied the width and height of the outer vestibule (shapes 1 and 2), length of the selectivity filter (shapes 3 and 4), width of the inner pore (shape 5), and the width of the intracellular pore (shapes 4, 6, and 7) and the width, and height of the outer vestibule and length of the selectivity filter simultaneously (shapes 8 and 9). We have maintained a fixed length of 54 Å for all channel shapes, as this is close to the length of the potassium channel.

VI. ACBD—ALGORITHMS

In the previous section, we formulated ACBD as a stochastic optimization problem (18) and provided two examples, namely PMF estimation of gramicidin channels and shape estimation of sodium channels. In this section, we focus on continuous and discrete stochastic optimization algorithms that optimize (18). Apart from Section VI-A, most of the discussion will focus on discrete stochastic optimization algorithms since they are of independent interest in the control of large scale dynamical systems.

A. Continuous Stochastic Optimization-Based ACBD Simulation Algorithm for PMF Estimation

Consider the PMF estimation problem for gramicidin formulated in Section V-B. Here, we parameterize the PMF U_θ in (5) by a finite-dimensional basis function representation with coefficients $\theta \in \Theta$ where $\Theta \subset \mathbb{R}^p$ is a compact set in Euclidean space. We then solve the

continuous stochastic optimization problem (18) to estimate the effective PMF. Recall $n = 0, 1, \dots$ denotes batch number.

Algorithm 2 Continuous ACBD Simulation Algorithm

Step 0: Set batch index $n = 0$, and initialize $\theta_0 \in \Theta$.
 Step 1 (Evaluation of loss function): At batch n , evaluate loss function $C_n(\theta_n)$ in (18) over the set of experimental conditions $\lambda \in \Lambda$. This involves computing $\hat{I}_n^{(\lambda)}(\theta)$ using the BD Algorithm 1.
 Step 2 (Gradient Estimation): Compute $\widehat{\nabla}_\theta C_n(\theta_n)$
 Step 3 (Stochastic Approximation Algorithm): Update PMF estimate

$$\theta_{n+1} = \theta_n - \epsilon_{n+1} \widehat{\nabla}_\theta C_n(\theta_n) \quad (23)$$

where ϵ_n denotes a decreasing step size (see discussion below for choice of step size).

Set n to $n + 1$ and go to Step 1.

The step size is typically chosen as $\epsilon_n = \epsilon / (n + 1 + R)^\kappa$, where $0.5 < \kappa \leq 1$ and R is some positive constant. This choice of step size satisfies the condition $\sum_{n=1}^{\infty} \epsilon_n = \infty$ which is required for convergence of Algorithm 2.

A crucial aspect of the algorithm is the gradient estimation Step 2. In this step, an estimate $\widehat{\nabla}_\theta C_n(\theta_n)$ of the gradient $\nabla_\theta C(\theta_n)$ is computed. This gradient estimate is then fed to the stochastic gradient algorithm (Step 3) which updates the PMF. Note that since the explicit dependence of $C_n(\theta_n)$ on θ is not known, it is not possible to analytically compute $\nabla_\theta C(\theta_n)$. Thus, we have to resort to gradient estimation. One can use a simple finite difference gradient estimator such as the Kiefer–Wolfowitz algorithm or Simultaneous Perturbation Stochastic Approximation (SPSA) algorithm; see [86] and the website <http://www.jhuapl.edu/SPSA/>. Alternatively, more sophisticated gradient estimators can be implemented such

as weak derivative estimators and Infinitesimal Perturbation Analysis (IPA) Estimators (see [87]), which typically have much smaller variances compared to finite difference methods.

Convergence of Controlled Brownian Dynamics Simulation Algorithm 2: By construction in Step 1 of Algorithm 2, for fixed θ , the loss function estimates $C_n(\theta)$ are independent and identically distributed random variables. Under this assumption, it is straightforward to prove that the estimates θ_n generated by ACBD Algorithm 2 (whether using the Kiefer–Wolfowitz or SPSA algorithm) converge to a local minimum of the loss function. We refer the reader to [26] for more sophisticated results that deal with convergence of stochastic gradient algorithms for state-dependent Markovian noise.

B. Discrete Stochastic Optimization-Based ACBD Simulation Algorithm

In the remainder of this section, we propose discrete stochastic optimization algorithms for shape estimation of sodium channels as well as PMF estimation of gramicidin channels (in this case, the parameter Θ in (22) comprised of the Gaussian means, variances, and weights is quantized to a finite set). For convenience of exposition, we will primarily refer to shape estimation in this section. Algorithms 4 and 5 are novel extensions of recent results in discrete stochastic optimization [88], [89] and are hence of independent interest. The algorithms have been used in other diverse applications ranging from optimization of wireless communication networks [90], [91] and experimental control of ion channels [92].

Because in actual BD simulations, the loss function $C_n(\theta)$ of (18) is nonnegative and uniformly bounded from above, it is convenient to normalize the objective (18) as follows. Let $\alpha \leq C_n(\theta) \leq \beta$, where α denotes a finite lower bound and $\beta > 0$ denotes a finite upper bound. For example, since $C_n(\theta)$ is nonnegative, α can be chosen as zero. Define the normalized costs $m_n(\theta)$ as

$$m_n(\theta) \triangleq \frac{C_n(\theta) - \alpha}{\beta - \alpha}, \quad \text{where } 0 \leq m_n(\theta) \leq 1. \quad (24)$$

Then, the stochastic optimization problem (18) is equivalent to

$$\theta^* = \arg \min_{\theta \in \Theta} m(\theta) \quad \text{where } m(\theta) \triangleq \mathbf{E}\{m_n(\theta)\} \quad (25)$$

since scaling the cost function does not affect the minimizing solution. Here, $\Theta = \{1, 2, \dots, S\}$ is a finite discrete set of possible shapes of the sodium channel.

Overview of Literature: There are several different classes of methods that can be used to solve the discrete stochastic optimization problem (25); see [88] and [93] for a recent survey. Problem (25) can also be viewed as a multi-armed bandit problem—which is a special kind of an infinite horizon Markov decision process with an “indexable” optimal policy [94]. In recent years, a number of discrete stochastic approximation algorithms have been proposed. Several of these algorithms [88], [95]–[99] including simulated annealing type procedures [100] and stochastic rulers [98] fall into the category of random search. In this paper, we construct algorithms based on the random search procedures in [95] and [96]. The basic idea is to generate a homogeneous Markov chain taking values in Θ which spends more time at the global optimum than at any other element of Θ .

An obvious brute force approach for computing the optimal ion channel shape θ^* is as follows. For each possible shape $\theta \in \Theta$, run the BD simulation Algorithm 1 for a very long sample size T and compute the estimated loss function $m_T(\theta)$ using (24) for each possible shape θ . Finally, pick $\hat{\theta}_T^* = \arg \min_{\theta \in \Theta} m_T(\theta)$. Since for any fixed θ , $m_T(\theta) \rightarrow m(\theta)$ with probability one (w.p. 1) as $T \rightarrow \infty$, it follows that the brute force estimator is statistically consistent, i.e., $\hat{\theta}_T^* \rightarrow \theta^*$ with probability one (w.p. 1) as $T \rightarrow \infty$. Thus, in principle, the above brute force simulation method can be used to compute the optimal channel shape. However, the method is highly inefficient since $m_T(\theta)$ needs to be evaluated for each $\theta \in \Theta$ via extensive BD simulation. The evaluations of $m_T(\theta)$ for $\theta \neq \theta^*$ are wasted because they contribute nothing to the estimation of the optimal shape. Indeed, the above brute force method was used manually in [85] to estimate the optimal channel shape—this took the authors several months.

The idea of discrete stochastic approximation [88], [90], [95], [96], [101], [102] is to run more BD simulations for θ , where the optimal shape is expected and less in other areas. More precisely, what is needed is a dynamic resource allocation (control) algorithm that controls (schedules) the BD simulation Algorithm 1 to efficiently estimate the optimal shape θ^* . We propose a discrete stochastic approximation algorithm that is both *consistent* and *attracted* to the optimal shape. That is, the algorithm provably spends more time at the optimal shape gathering observations $\hat{I}^{(\lambda)}(\theta)$ at the optimal shape $\theta = \theta^*$ and less time for other shapes $\theta \in \Theta$. Thus, in discrete stochastic approximation the aim is to devise an *efficient* [87, Ch. 5.3] adaptive search (sampling plan) which allows us to find the minimizer θ^* with as few samples as possible by not making unnecessary observations at nonpromising values of θ .

1) *Discrete Stochastic Approximation ACBD Algorithm:* In the algorithm that follows, the process $\{\theta_n, n = 1, 2, \dots\}$ denotes the “state” of the algorithm. For the state θ_n , at

batch time n , define the neighborhood set $\mathcal{N}_{\theta_n} = \Theta - \{\theta_n\}$. Finally, denote the S -dimensional standard unit vectors by \mathbf{e}_m , $m = 1, \dots, S$, where $\mathbf{e}_m = [0 \ \dots \ 0 \ 1 \ 0 \ \dots \ 0]'$ with 1 in the m th position and zeros elsewhere.

Consider the following algorithm.

Algorithm 3 Stochastic Search ACBD Algorithm for Ion Channel Shape Estimation

Step 0: (Initialization.) At batch-time $n = 0$, initialize state of the algorithm $\theta_0 \in \{1, \dots, S\}$ randomly. Initialize state occupation probabilities $\pi_0 = \mathbf{e}_{\theta_0}$. Initialize optimal shape estimate of ion channel as $\theta_0^* = \theta_0$.

Step 1: (Sampling and exploration.) At batch n , given current algorithm state θ_n , evaluate $m_n(\theta_n)$ according to (24) by conducting Λ independent BD simulation runs of Algorithm 1 on the ion channel.

Generate an alternative candidate state $\tilde{\theta}_n$ by sampling uniformly from the neighborhood \mathcal{N}_{θ_n} of current state θ_n . Evaluate $m_n(\tilde{\theta}_n)$.

Step 2: (Conditional acceptance test.) If $m_n(\tilde{\theta}_n) < m_n(\theta_n)$, set $\theta_{n+1} = \tilde{\theta}_n$, else, set $\theta_{n+1} = \theta_n$.

Step 3: Update empirical state occupation probabilities π_n as

$$\pi_{n+1} = \pi_n + \mu_n(\mathbf{e}_{\theta_{n+1}} - \pi_n), \quad \pi_0 = \mathbf{e}_{\theta_0}. \quad (26)$$

Step 4: (Update estimate of shape of ion channel.) $\theta_n^* = \tilde{\theta}(m^*)$ where $m^* = \arg \max_{m \in \{1, \dots, S\}} \pi_{n+1}(m)$, set $n \rightarrow n + 1$, go to Step 1.

Remark: The elements $\pi_n(\theta)$ of π_n generated by Step 3 are merely normalized counters for how many times the algorithm state has visited any particular shape $\theta \in \Theta$. In particular

$$\pi_n(\theta) = \frac{\# \text{ of times state visits shape } \theta \text{ in batches 1 to } n}{n} \quad (27)$$

is the empirical occupation probability of state θ . As we will show, the attraction capability (efficiency) of Algorithm 3 is captured by the fact that for sufficiently larger n , $\pi_n(\theta^*) > \pi_n(\theta)$, meaning that the algorithm spends more time at the optimal shape θ^* than at any other shape $\theta \in \Theta$. As a consequence, θ_n^* (which according to Step 4 is the shape at which the algorithm has spent maximum time until time n) converges to the optimal shape θ^* with probability one. This is formalized as follows.

Convergence of Algorithm 3: In [96], the following stochastic ordering assumption is used:

(O) For each $\theta, \tilde{\theta} \in \Theta$,

$$P(m_n(\theta^*) < m_n(\theta)) \geq P(m_n(\theta) > m_n(\theta^*))$$

$$P(m_n(\tilde{\theta}) > m_n(\theta^*)) \geq P(m_n(\tilde{\theta}) > m_n(\theta)).$$

Roughly speaking, this assumption ensures that the algorithm is more likely to jump towards a global minimum than away from it, see [96] for details.

The following convergence theorem for Algorithm 3 is proved in [96].

Theorem 2 (Convergence and Efficiency of Algorithm 3): Under condition (O), the estimated sequence $\{\theta_n^*\}$ generated by Step 4 of Algorithm 3 converges with probability one to the global optimizer θ^* . Equivalently, Algorithm 3 is attracted to θ^* in that for sufficiently large n , the state spends more time at θ^* than any other value of $\theta \in \Theta$, i.e., the state occupation probabilities generated by Step 3 (26) satisfy $\pi_n(\theta^*) > \pi_n(\theta)$, $\theta \in \Theta - \{\theta^*\}$.

A sufficient condition for Assumption (O) to hold (see [96]) is that the probability density function of the mean square error current $m_n(\theta)$ is symmetric, unimodal, and identical for all $\theta \in \Theta$. Since the distribution of the mean square error current $m_n(\theta)$ is not known, it is difficult to verify Assumption (O). However, Algorithm 3 yields excellent numerical results for estimating the shape of the sodium channel (Section VII).

2) *Discrete Search/Ruler-Based ACBD Algorithm:* We propose two alternative discrete stochastic optimization algorithms that require much less restrictive conditions for convergence than Algorithm 3. We start by expressing the optimal ion channel shape θ^* as the solution of the following equivalent stochastic optimization problem. Define the loss function

$$Y_n(\theta, u_n) = \mathbf{I}(m_n(\theta) - u_n) \quad (28)$$

where $\mathbf{I}(x) = \begin{cases} 1, & \text{if } x > 0 \\ 0, & \text{otherwise.} \end{cases}$

Here, u_n is an independent uniform random number in $[0, 1]$. The uniform random number u_n is a stochastic ruler against which the candidate $m_n(\theta)$ is measured. The result was originally used in devising stochastic ruler optimization algorithms [89]; although, here we propose a more efficient algorithm than the stochastic ruler. Applying Algorithm 3 to the cost function $\mathbf{E}\{Y_n(\theta, u_n)\}$ defined in (28) yields the following search-ruler algorithm.

Algorithm 4 Stochastic Search Ruler-Based ACBD Algorithm for Ion Channel Shape Estimation

Identical to Algorithm 3 with $m_n(\theta_n)$ and $m_n(\tilde{\theta}_n)$ replaced by $Y_n(\theta_n, u_n)$ and $Y_n(\tilde{\theta}_n, \tilde{u}_n)$. Here u_n and \tilde{u}_n are independent uniform random numbers.

Theorem 3 (Convergence and Efficiency of Algorithm 4): The estimated sequence $\{\theta_n^*\}$ generated by Step 4 of the search ruler Algorithm 4 converges with probability one to the global optimizer θ^* . Equivalently, Algorithm 4 is attracted to θ^* in that for sufficiently large n , the state spends more time at θ^* than any other value of $\theta \in \Theta$, i.e., the state occupation probabilities generated by Step 3 (26) satisfy $\pi(\theta^*) > \pi(\theta)$, $\theta \in \Theta - \{\theta^*\}$. Here

$$\lim_{n \rightarrow \infty} \frac{\pi_n(\theta^*)}{\pi_n(\theta)} = \frac{\pi(\theta^*)}{\pi(\theta)} = \frac{m(\theta)}{m(\theta^*)} \frac{(1 - m(\theta^*))}{(1 - m(\theta))} > 1. \quad (29)$$

The proof is presented in Appendix.

Discussion: Inequality (29) gives an explicit representation of the discriminative power of the algorithms between the optimum shape θ^* and any other candidate θ in terms of the normalized expected costs $m(\theta)$ and $m(\theta^*)$. Algorithm 4 is more efficient than the stochastic ruler algorithm of [88] when the candidate samples are chosen with equal probability. The stochastic ruler algorithm of [88] has asymptotic efficiency $\pi(\theta^*)/\pi(\theta) = (1 - m(\theta^*))/(1 - m(\theta))$. So, Algorithm 4 has the additional improvement in efficiency due to the additional multiplicative term $m(\theta)/m(\theta^*)$ in (29).

C. Search Ruler With Antithetic Variable Variance Reduction

A more efficient implementation of the search-ruler Algorithm 4 can be obtained by using variance reduction based on antithetic variables as follows. Since u_n is uniformly distributed in $[0, 1]$, so is $1 - u_n$. Similar to Theorem 3, it can be shown that the optimal ion channel shape θ^* defined in (25) is the minimizing solution of the following stochastic optimization problem $\theta^* = \arg \min_{\theta} \mathbf{E}\{Z_n(\theta, u_n)\}$ where

$$Z_n(\theta, u_n) = \frac{1}{2} [Y_n(m_n(\theta), u_n) + Y_n(m_n(\theta), 1 - u_n)] \quad (30)$$

where the normalized sample cost $m_n(\theta)$ is defined in (25). Since the indicator function $\mathbf{I}(\cdot)$ is a monotonic function of its argument, the following well-known result in antithetic variables applies; see [103, p. 136] for proof.

Result 4: For the variables Z_n in (30) and Y_n in (28), $\text{var}\{Z_n(\theta, u_n)\} \leq \text{var}\{Y_n(\theta, u_n)\}$.

As a result, one would expect that the stochastic optimization algorithm using Z_n would converge faster. Applying Algorithm 4 to the cost function $\mathbf{E}\{Z_n(\theta)\}$ defined in (30) yields the variance reduced search-ruler algorithm.

D. Kernel-Based Constrained Exploration Exploitation

The above discrete ACBD algorithms can be modified to dynamically adapt their exploration of the possible shapes as the number of iterations increases. Typically, during initial iterations of a learning algorithm, it is desirable to aggressively explore more candidates since one is uncertain how good the current estimate is. After more confidence has been obtained about the candidates, it is desirable to reduce exploration and exploit the best candidates. This adaptation is done via a kernel-based learning algorithm. The key idea is Step 3, where a kernel-based update is used.

Algorithm 5 Kernel-Based Adaptive Exploration/Exploitation ACBD Algorithm

Step 0: Identical to Algorithm 3.

Step 1: (Adaptive Sampling and Exploration.) Evaluate $m_n(\theta_n)$. Then perform the following two level sampling procedure: Simulate a Bernoulli random variable $\gamma_n \in \{0, 1\}$ with probabilities $P(\gamma_n = 0) = 2\alpha_n$ and $P(\gamma_n = 1) = 1 - 2\alpha_n$, where $0 \leq \alpha_n \leq 1/2$.

- If $\gamma_n = 0$, perform exploration as follows: sample $\tilde{\theta}_n$ uniformly from \mathcal{N}_{θ_n} . Evaluate $m_n(\tilde{\theta}_n)$ and go to Step 2.

- If $\gamma_n = 1$ (perform no exploration), go to Step 3.

Step 2: (Conditional Acceptance test.) If $m_n(\tilde{\theta}_n) < m_n(\theta_n)$, set $\theta_{n+1} = \tilde{\theta}_n$, else, set $\theta_{n+1} = \theta_n$.

Step 3: (Update Kernel-based exploration probability α_n and state occupation probabilities π_n .)

$$\pi_{n+1} = \pi_n + \mu_n (\mathbf{e}_{\theta_{n+1}} - \pi_n), \quad \pi_0 = \mathbf{e}_{\theta_0} \quad (31)$$

$$T_{n+1} = T_n + \mu_n (\mathbf{e}_{\theta_{n+1}} - \pi_n - T_n) \quad (32)$$

$$\alpha_{n+1} = 0.5 \left[1 - K \left(\frac{T_{n+1}}{\delta_{n+1}} \right) \right] \quad (33)$$

where $\delta_n \geq 0$, $\delta_n \rightarrow 0$, and $\mu_n/\delta_n \rightarrow 0$ as $n \rightarrow \infty$.

Step 4: Identical to Algorithm 3.

In the above algorithm, for any $x \in \mathbb{R}^S$ the kernel

$$K(x) = \begin{cases} (1 - x'x), & \text{if } \|x\|_2 = \sqrt{x'x} \leq 1 \\ 0, & \text{otherwise.} \end{cases}$$

The intuition in the above kernel-based learning in Step 3 is as follows. In early iterations the algorithm knows little about the optimal shape. Hence, the average error T_n between e_{θ_n} and the empirical occupation π_n is large. When this average error T_n is large, then $K(T_{n+1}/\delta_n)$ is close to zero and α_n given in (33) is close to 0.5. Thus, in early iterations the algorithm is forced to explore the space of candidate shapes. As the iterations progress and the algorithm learns the optimal shape, the average error T_n is getting smaller, then $K(T_{n+1}/\delta_n)$ is close to one and $\alpha_n \rightarrow 0$. As a result, as the algorithm becomes more confident about the optimal shape estimate, it reduces the exploration probability to reduce the exploration cost.

Remark: Corresponding versions for Algorithm 4 and its antithetic variable variance reduced version are obtained by replacing $m_n(\theta)$ by $Y_n(\theta, u_n)$ and $Z_n(\theta, u_n)$.

The following theorem deals with the convergence of the above algorithm. The proof is presented in [92].

Theorem 5: Assume that the conditions of Theorem 2 are satisfied. Then, the sequence $(\pi_n, T_n, \alpha_n)'$ given in Step 3 above converges to $(\pi, 0, 0)'$ w.p. 1. Also, Algorithm 5 is attracted to the equilibrium potential θ^* .

Theorem 5 says that the exploration probability α_n converges to zero. This is intuitively appealing since it means that as the algorithm becomes more confident in its estimate of the optimal candidate, fewer computational resources are spent running BD algorithms on other less promising candidates. We refer the reader to [92] for further motivation of the above adaptive kernel learning algorithm. The rate of convergence of the algorithm is studied in [92] by use of diffusion approximation methods; see also [104, Ch. 10].

VII. NUMERICAL EXAMPLES

The ACBD simulation algorithms were run on the Linux Cluster LC supercomputer of the Australian National University Supercomputer Facility at the Glacier supercomputer at the University of British Columbia, Canada (which is part of the Westgrid network). Glacier is comprised of 840 dual processor nodes, each node being an IBM blade Xeon 3.06 GHz processor.

A. Example 1: Estimating PMF of Gramicidin Ion Channels

Here, we illustrate the performance of discrete stochastic optimization-based ACBD Algorithm 3 in estimating the PMF of a gramicidin channel formulated in Section V-B. Further detailed numerical results are presented in [105]. Consider the parameterization $\theta = (W, \sigma^2, m, \sigma_0^2, m_0)'$ defined in (21) for the PMF U_θ . Since the positions of the potential wells for the gramicidin

channel are known to be around -9 \AA and $+9 \text{ \AA}$ [25], [78], we fix the components $W = 9$, $\sigma^2 = 16$, and $\sigma_0^2 = 12.25$ in θ . In our numerical study, we have assumed, for simplicity, prior knowledge of the position and number of binding sites. Note that this assumption is not essential since our algorithm can also estimate these parameters. Thus, our aim is to estimate the two components (m, m_0) which determines the depth of the two potential wells of the gramicidin channel and the height of the potential barrier between the wells. This is obtained by estimating the parameter θ^* that optimizes the fit between the BD simulated current and experimentally determined current. We thus construct Θ_d to contain 25 possible values for (m, m_0) corresponding to well depth $\in \{5 \text{ kT}, 6 \text{ kT}, 7 \text{ kT}, 8 \text{ kT}, 9 \text{ kT}\}$ and barrier height $\in \{4 \text{ kT}, 4.5 \text{ kT}, 5 \text{ kT}, 5.5 \text{ kT}, 6 \text{ kT}\}$. The particular values of these parameters were chosen after a preliminary study showed that choices of well-depth and barrier-height outside the given range lead to significant degradation in performance; we thus find the best fit PMF from this subset which comprises a reasonable range of values.

Each iteration runs 24 BD algorithms in parallel (12 experimental conditions for θ_n and $\tilde{\theta}_n$ in Step 1 of the adaptive BD) on the supercomputer. The experimentally determined current $I(\lambda)$ is evaluated at 12 different

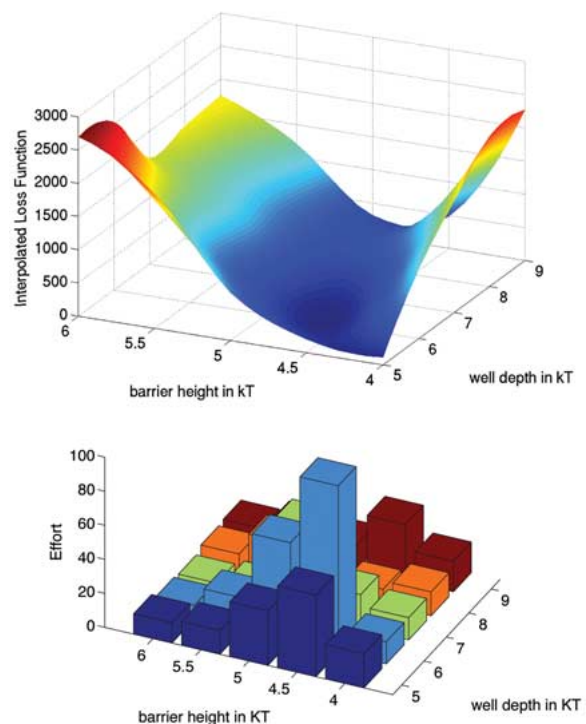


Fig. 8. Figure depicts error surface $C(\theta)$ for PMF estimate of gramicidin channel. Minimum is at a well depth of 6 kT and barrier height of 4.5 kT.

Table 2 Simulation Conditions: Simulations Were Performed for Each Shape With All 12 Conditions. Concentrations Inside and Outside the Channels Were Varied Between Solutions of NaCl and CaCl₂ and Both. External Potentials of ±70 and ±100 mV Were Applied

Condition	Ion Type	Φ^{ext} (mV)	Experimental \hat{I} (pA)	Internal Conc.(mM)	External Conc.(mM)	No. of Ions in R_1	No. of Ions in R_2
1	NaCl	+100	+2.3	200	200	14	14
2	NaCl	-100	-2.3	200	200	14	14
3	CaCl ₂	-100	0.0	200	200	8	8
4	NaCl	-100	-0.5	200	200	12	12
	CaCl ₂			100	100	6	6
5	NaCl	+100	+1.2	200	200	12	12
	CaCl ₂			100	100	6	6
6	NaCl	-70	-1.6	200	200	14	14
7	NaCl	+70	+1.6	200	200	14	14
8	NaCl	-70	-1.45	100	100	10	10
9	NaCl	+70	+1.45	100	100	10	10
10	NaCl	-70	-1.65	350	350	16	16
11	NaCl	-70	-0.4	200	200	12	12
	CaCl ₂			100	100	7	0
12	NaCl	+70	+0.9	200	200	12	12
	CaCl ₂			100	100	0	7

voltages and concentrations on the current–voltage–concentration profiles of the gramicidin channel. The concentration–voltage pairs used cover voltages ranging from 25–200 mV at a concentration of 500 mM as well as concentrations ranging from 100–1000 mM at voltages of 100 and 200 mV. Specifically, the conditions we used are 25, 50, 75, 100, 150, and 200 mV from the current–voltage curve obtained with an ionic concentration of 500 mM; 100, 200, 500, and 1000 mM from the current–concentration curves were obtained with the applied potentials of 100 and 200 mV.

Moreover, Fig. 8 illustrates the profile of the loss function obtained using Algorithm 3 with the varying well depths and barrier heights in Θ_d as well as an interpolated version of this surface. The figure shows that the optimal value for the loss function (in dark blue) occurs at well depth and barrier height of 6 kT and 4.5 kT as mentioned previously. It also suggests that there are several possible PMF parameter values that produce near optimal values for the loss function.

B. Example 2: Shape Estimation of Sodium Channels

Here, we illustrate the performance of Algorithm 3 in estimating the shape of the sodium channel. In the BD simulations we match the BD current $\hat{I}^{(\lambda)}(\theta)$ to 12 different experimental conditions $\lambda \in \Lambda$ where $\Lambda = \{\lambda_1 \dots \lambda_{12}\}$. These are described in Table 2 where each condition corresponds to one value for λ . The experimental currents $I^{(\lambda)}$ used to match our simulation currents are from experimental data in [106]–[108] for actual sodium channels under different experimental conditions. It took approximately 38 h of simulation time to simulate all the experimental conditions $\lambda \in \Lambda$ at each $n \in N$ and a total of approximately ~4500 h for 120 batches. With batch jobs

running in parallel, it took less than three weeks to obtain all the results.

Fig. 9 shows the cost $C(\theta)$ for the nine different shapes. It also shows the effort Algorithm 3 spends on the different candidates. Fig. 9 also plots the empirical occupation probabilities π_n at iteration $n = 120$ for Algorithm 3. The plot illustrates the attraction property of the algorithm. It spends more time at the optimal shape (Case 4) than any other shape. The closest candidate shape to Case 4 is Case 1 and the figures shows that the algorithm spends the second largest time at Case 1.

Discussion: The reason why the loss function for shape $\theta = 4$ and $\theta = 1$ are very similar can be explained as follows. From Table 1, the only difference between the two shapes is the diameter of the outer vestibule. In this region, the ions filling up this external vestibule are responsible for aiding the ions further in the selectivity filter to conduct through the channel by providing them with a repulsive kick. For shape $\theta = 1$ the width of this region is nearly 28 Å, and for shape $\theta = 4$ it is only about 14 Å. There are no other differences between the two models. We know from [85] that this outer vestibule region contains on average about two ions during much of the BD simulation. What we have learned from this new set of simulations performed with Algorithm 2, is that, as long as the vestibule is wide enough to accommodate two ions, its exact width seems to be irrelevant. Once the two ions are present in this outer vestibule, the ions inside the channel are provided with enough repulsive force for these resident ions to move through to the other side of the channel. Thus, even though it might seem that two shapes were selected by the algorithm as being almost equally successful in satisfying all the experimental

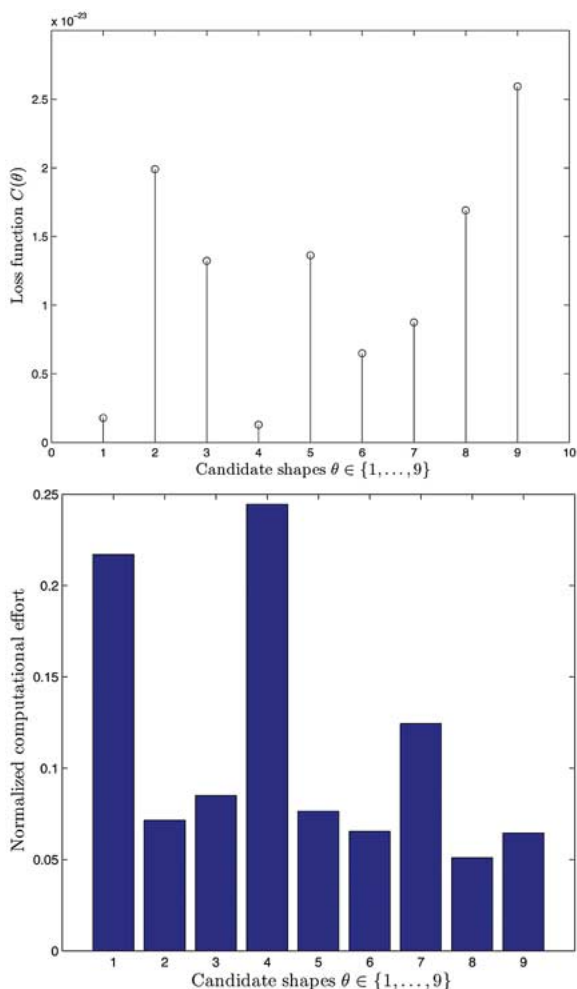


Fig. 9. (a) Error surface $C(\theta)$ for nine different shapes for sodium channel. (b) Computational effort spent on the nine different candidates by ACBD discrete optimization Algorithm 3. Figure shows attraction property of Algorithm 3 to optimal shape—algorithm spends more effort at optimal shape compared to other shapes.

conditions presented, the important features for selectivity and permeation in the sodium channel are still maintained.

VIII. CONCLUDING REMARKS

In this paper, we have given a detailed description of the permeation problem in biological membrane ion channels. The main theme of this paper is the formulation of the ion channel permeation problem as a large scale interacting particle dynamical system comprised of ions, protein atoms, and water molecules.

In Section II, we discussed four widely used physical models for ion channel permeation, namely quantum mechanics, MD, BD, and PNP theory. Of these four theories for permeation, as discussed in Section II, BD is

computationally tractable and yet sufficiently accurate for modeling ion permeation in many important biological ion channels.

In Section IV, we presented a detailed description of BD. In BD, the propagation of ions in the ion channel is modeled as a large-scale, multiparticle, continuous-time, stochastic dynamical system satisfying the Langevin equation. The key idea here is that instead of considering the dynamics of individual water molecules, which is computationally intractable, the BD system considers the average effect of water molecules as a random force acting on individual ions. We also presented a probabilistic interpretation of BD.

One of the major caveats to using BD in studying the permeation dynamics in biological ion channels is the use of Poisson's equation to calculate the forces encountered by permeant ions. The issue here is whether one can legitimately employ macroscopic electrostatics in regions that are not much larger than the diameters of the water molecules and ions. In the narrow, constricted region of the channel, such as in the selectivity filter of the potassium channel, the representation of the channel contents as a continuous medium is a poor approximation. The method of ACBD, which we discussed in Sections V and VI, is designed to circumvent the limitations posed in the conventional simulation approach. Using the ACBD algorithm, we are able to solve the inverse problem. That is, given the 3-D shape of a channel, we can deduce the potential of mean force encountered by an ion traversing the channel that correctly replicates experimental findings, thus obviating the need to solve Poisson's equation. Another issue with BD is the replacement of ions to maintain the fixed concentration; see remark following Procedure 1 in Section III-D. We refer to [109] and [110] for further discussion.

Since ions are assumed to be spherically symmetric, the BD formulation in this paper only considers translational movement (2) and velocity (3). However, drug and channel blocker molecules are large and asymmetric. To model the effect of such large asymmetric molecules on ion channel permeation, it is necessary to consider both translational as well as rotational dynamics in a BD formulation [111]. Such a methodology may be used to explain how such drugs/blockers interact dynamically and bind with the ion channel. Understanding the dynamics of such a mechanism at a molecular level can eventually lead to the design of more efficient drugs and channel blockers. ■

APPENDIX

Proof of Theorem 3

We first show that the optimal ion channel shape θ^* defined in (25) is the minimizing solution of the following stochastic optimization problem $\theta^* = \arg \min_{\theta} \mathbf{E}\{Y_n(\theta, u_n)\}$.

The proof is as follows: Using the smoothing property of conditional expectations yields

$$\begin{aligned} \mathbf{E}\{\mathbf{I}(m_n(\theta) - u_n)\} &= \mathbf{E}\{\mathbf{E}\{\mathbf{I}(m_n(\theta) - u_n) | m_n(\theta)\}\} \\ &= \mathbf{E}\{P(u_n < m_n(\theta))\} \\ &= \mathbf{E}\{m_n(\theta)\} \\ &= m(\theta). \end{aligned}$$

The second equality follows since expectation of an indicator function is probability, and the third equality holds because u_n is a uniform random number in $[0, 1]$ so that $P(u_n < a) = a$ for any a in $[0, 1]$.

Next, we show that the state process $\{\theta_n\}$ generated by Algorithm 4 is a homogeneous, aperiodic, irreducible, Markov chain on the state space Θ with transition probability matrix $A = (a_{ij}, i, j \in \Theta)$ where

$$a_{ij} = P(\theta_n = j | \theta_{n-1} = i) = \frac{1}{S-1} m(i)(1 - m(j)). \quad (34)$$

That the process $\{\theta_n\}$ is a homogeneous aperiodic irreducible Markov chain follows from its construction in Algorithm 4—indeed θ_n only depends probabilistically on θ_{n-1} . From Algorithm 4, given candidate i and its

associated cost $Y_n(i, u_n)$, candidate j is accepted if its associated cost $\tilde{Y}_n(j, \tilde{u}_n)$ is smaller. So, the probability of the algorithm transitioning from state i to state j is

$$\begin{aligned} a_{ij} &= \frac{1}{S-1} P(\tilde{Y}_n(j, \tilde{u}_n) < Y_n(i, u_n)) \\ &= \frac{1}{S-1} P(m_n(j) < \tilde{u}_n) P(m_n(i) > u_n). \end{aligned}$$

Finally, it is straightforward to verify that

$$\pi(\theta) = c(1 - m(\theta)) \prod_{j \neq \theta} m(j) \quad (35)$$

satisfies the invariant distribution where c denotes a normalization constant. Hence

$$\frac{\pi(\theta^*)}{\pi(\theta)} = \frac{m(\theta)(1 - m(\theta^*))}{m(\theta^*)(1 - m(\theta))} = \frac{1/m(\theta^*) - 1}{1/m(\theta) - 1}$$

which is clearly ≥ 1 since $m(\theta^*)$ is the global minimum; therefore, $m(\theta^*) \leq m(\theta)$.

REFERENCES

- [1] F. Ashcroft, *Ion Channels and Disease*. New York: Academic, 2000.
- [2] V. Krishnamurthy, S. H. Chung, and G. Dumont, Eds., *Ion Channels: Bio Nanotubes—Special Issue of IEEE Trans. NanoBioScience*. Piscataway, NJ: IEEE Press, Mar. 2005, vol. 4.
- [3] S. H. Chung, O. Andersen, and V. Krishnamurthy, Eds., *Biological Membrane Ion Channels: Dynamics, Structure and Applications*. New York: Springer-Verlag, 2006.
- [4] B. Hille, *Ionic Channels of Excitable Membranes*, 3rd ed. Sunderland, MA: Sinauer, 2001.
- [5] T. W. Allen, T. Bastug, S. Kuyucak, and S. H. Chung, “Gramicidin A channel as a test ground for molecular dynamics force fields,” *Biophys. J.*, vol. 84, pp. 2159–2168, 2003.
- [6] M. O’Mara, P. H. Barry, and S. H. Chung, “A model of the glycine receptor deduced from Brownian dynamics studies,” in *Proc. Nat. Acad. Sci. USA*, 2003, vol. 100, no. 4310–4315.
- [7] D. Doyle, J. Cabral, R. Pfuetzner, A. Kuo, J. Gulbis, S. Cohen, B. Chait, and R. MacKinnon, “The structure of the potassium channel: Molecular basis of K^+ conduction and selectivity,” *Science*, vol. 280, pp. 69–77, 1998.
- [8] R. Dutzler, E. Campbell, M. Cadene, B. Chait, and R. MacKinnon, “X-ray structure of a CIC chloride channel at 3.0 Å reveals the molecular basis of anion selectivity,” *Nature*, vol. 415, pp. 287–294, 2002.
- [9] R. Dutzler, E. Campbell, and R. MacKinnon, “Gating the selectivity in CIC chloride channels,” *Science*, vol. 300, pp. 108–112, 2003.
- [10] R. Bass, P. Stropo, M. Baraclay, and D. C. Reece, “Crystal structure of *Escherichia coli* MscS, a voltage-modulated and mechanosensitive channel,” *Science*, vol. 298, pp. 1582–1587, 2002.
- [11] S. Long, E. B. Campbell, and R. MacKinnon, “Crystal structure of a mammalian voltage-dependent *Shaker* family K^+ channel,” *Science*, vol. 309, pp. 897–903, 2004.
- [12] S. Long, E. B. Campbell, and R. MacKinnon, “Voltage sensor of Kv1.2: Structural basis of electromechanical coupling,” *Science*, vol. 309, pp. 897–903, 2004.
- [13] N. Unwin, “Refined structure of the nicotinic acetylcholine receptor at 4 Å resolution,” *J. Molecular Biol.*, vol. 346, pp. 967–989, 2005.
- [14] S. H. Chung and S. Kuyucak, “Recent advances in ion channel research,” *Biochimica et Biophysica Acta*, vol. 1565, pp. 267–286, 2002.
- [15] R. Eisenberg, “From structure to function in open ionic channels,” *J. Membrane Biology*, vol. 171, pp. 1–24, 1999.
- [16] B. Roux, S. Bernéche, and W. Im, “Ion channels, permeation, and electrostatics: Insight into the function of KcsA,” *Biochemistry*, vol. 39, pp. 13 295–13 306, 2000.
- [17] D. Tieleman, P. Biggin, G. Smith, and M. Sansom, “Simulation approaches to ion channel structure-function relationships,” *Quarterly Rev. Biophys.*, vol. 34, pp. 473–561, 2001.
- [18] M. Jackson, *Molecular and Cellular Biophysics*. Cambridge, U.K.: Cambridge Univ. Press, 2006.
- [19] V. Krishnamurthy and S. H. Chung, “Brownian dynamics simulation for modeling ion permeation across bio-nanotubes,” *IEEE Trans. Nanobiosci.*, vol. 4, no. 1, pp. 102–111, Mar. 2005.
- [20] V. Krishnamurthy and S. H. Chung, “Adaptive Brownian dynamics simulation for estimating potential of mean force in ion channel permeation,” *IEEE Trans. Nanobiosci.*, vol. 5, no. 2, pp. 126–138, Jun. 2006.
- [21] S. Kuyucak, O. Andersen, and S. H. Chung, “Models of permeation in ion channels,” *Rep. Progress Phys.*, vol. 64, pp. 1427–1472, 2001.
- [22] A. Grottesi, C. Domene, S. Haider, and M. S. P. Sansom, “Molecular dynamics simulation approaches to k channels: Conformational flexibility and physiological function,” *IEEE Trans. Nanobiosci.*, vol. 4, no. 1, pp. 112–120, May 2005.
- [23] S. Edwards, B. Corry, S. Kuyucak, and S. H. Chung, “Continuum electrostatics fails to describe ion permeation in the gramicidin channel,” *Biophys. J.*, vol. 83, pp. 1348–1360, Sep. 2002.
- [24] S. Noskov, S. Yu, S. Bernéche, and B. Roux, “Control of ion selectivity in potassium

- channels by electrostatic and dynamic properties of carbonyl ligands," *Nature*, vol. 431, pp. 830–834, 2004.
- [25] T. Allen, O. S. Andersen, and B. Roux, "On the importance of atomic fluctuations, protein flexibility, and solvent in ion permeation," *J. General Physiol.*, vol. 124, pp. 679–690, 2004.
- [26] H. Kushner and G. Yin, *Stochastic Approximation Algorithms and Applications*. New York: Springer-Verlag, 1997.
- [27] H. Kushner, *Approximation and Weak Convergence Methods for Random Processes, With Applications to Stochastic Systems Theory*. Cambridge, MA: MIT Press, 1984.
- [28] V. Solo and X. Kong, *Adaptive Signal Processing Algorithms—Stability and Performance*. Englewood Cliffs, NJ: Prentice-Hall, 1995.
- [29] D. Chen and R. Eisenberg, "Charges, currents, and the potentials in ionic channels of one conformation," *Biophys. J.*, vol. 64, pp. 1405–1421, 1993.
- [30] R. Eisenberg, "Computing the field in proteins and channels," *J. Membrane Biology*, vol. 150, pp. 1–25, 1996.
- [31] B. Nadler, Z. Schuss, A. Singer, and R. Eisenberg, "Ionic diffusion through confined geometries: From Langevin equations to partial differential equations," *J. Phys.: Condensed Matter*, vol. 16, pp. S2153–S2165, 2004.
- [32] R. Coalson and M. Kurnikova, "Poisson-Nernst-Planck theory approach to the calculation of current through biological ion channels," *IEEE Trans. Nanobiosci.*, vol. 4, no. 2, pp. 263–277, May 2005.
- [33] P. Jordan, "Ion permeation and chemical kinetics," *J. General Physiol.*, vol. 114, pp. 601–604, 1999.
- [34] J. Alvarez and B. Hajek, "Equivalence of trans paths in ion channels," *Phys. Rev. E*, vol. 73, 2006.
- [35] Chemistry at HARvard Macromolecular Mechanics (CHARMM). [Online]. Available: <http://www.charmm.org>
- [36] T. Allen, S. Kuyucak, and S. H. Chung, "Molecular dynamics estimate of ion diffusion in model hydrophobic and the KcsA potassium channel," *Biophys. Chem.*, vol. 86, pp. 1–14, 2000.
- [37] S. Wan, C. Wang, and Y. Shi, "Generalized Langevin dynamics simulation," *Molecular Phys.*, vol. 93, no. 6, pp. 901–912, 1998.
- [38] T. Bastug and S. Kuyucak, "Memory effects in Brownian dynamics simulations of ion transport," *Chemical Phys. Lett.*, vol. 401, pp. 175–179, 2005.
- [39] P. E. Kloeden and E. Platen, *Numerical Solution of Stochastic Differential Equations*. Berlin, Germany: Springer, 1992.
- [40] W. V. Gunsteren, H. Berendsen, and J. Rullmann, "Stochastic dynamics for molecules with constraints Brownian dynamics of n-alkalines," *Molecular Phys.*, vol. 44, no. 1, pp. 69–95, 1981.
- [41] S. Bek and E. Jakobsson, "Brownian dynamics study of a multiply occupied cation channel: Application to understanding permeation in potassium channel," *Biophys. J.*, vol. 66, pp. 1028–1038, 1994.
- [42] K. Cooper, E. Jakobsson, and P. Wolynes, "The theory of ion transport through membrane channels," *Progress Biophys. Molecular Biology*, vol. 46, pp. 51–96, 1985.
- [43] E. Jakobsson and S. Chiu, "Stochastic theory of ion movement in channels with single-ion occupancy. Application to sodium permeation of gramicidin channels," *Biophys. J.*, vol. 52, pp. 33–45, 1987.
- [44] S. H. Chung, T. Allen, M. Hoyles, and S. Kuyucak, "Permeation of ions across the potassium channel: Brownian dynamics studies," *Biophys. J.*, vol. 77, pp. 2517–2533, 1999.
- [45] B. Corry, T. Allen, S. Kuyucak, and S. H. Chung, "Mechanisms of permeation and selectivity in calcium channels," *Biophys. J.*, vol. 80, pp. 195–214, Jan. 2001.
- [46] S. Datta, *Quantum Transport, Atom to Transistor*. Cambridge, MA: Cambridge Univ. Press, 2005.
- [47] F. Stillinger and A. Rahman, "Improved simulation of liquid water by molecular dynamics," *J. Chemical Phys.*, vol. 60, pp. 1545–1557, 1974.
- [48] E. Guàrdia, R. Rey, and J. Padró, "Potential of mean force by constrained molecular dynamics: A sodium chloride ion-pair in water," *J. Chemical Phys.*, vol. 155, pp. 187–195, 1991.
- [49] E. Guàrdia, R. Rey, and J. Padró, "Na⁺ – Na⁺ and Cl⁻ – Cl⁻ ion pairs in water: Mean force potentials by constrained molecular dynamics," *J. Chemical Phys.*, vol. 95, pp. 2823–2831, 1991.
- [50] I. Gihman and A. Skorohod, *Stochastic Differential Equations*. Springer-Verlag, 1972.
- [51] R. Eisenberg, M. Klosek, and Z. Schuss, "Diffusion as a chemical reaction: Stochastic trajectories between fixed concentrations," *J. Chemical Phys.*, vol. 102, pp. 1767–1780, 1995.
- [52] C. Schultz and A. Warshel, "What are the dielectric 'constants' of proteins and how to validate electrostatic models?" *Proteins*, vol. 44, pp. 400–417, 2001.
- [53] P. Smith, R. M. Brunne, A. E. Mark, and W. F. van Gunsteren, "Dielectric properties of trypsin inhibitor and lysozyme calculated from molecular dynamics simulations," *J. Physical Chemistry*, vol. 97, pp. 2009–2014, 1993.
- [54] T. Simonson and C. Brooks, III, "Charge screening and the dielectric constant of proteins: Insights from molecular dynamics," *J. Amer. Chem. Soc.*, vol. 118, pp. 8452–8458, 1996.
- [55] J. Pitera, M. Falta, and W. van Gunsteren, "Dielectric properties of proteins from simulation: The effects of solvent, ligands, pH, and temperature," *Biophys. J.*, vol. 80, pp. 2546–2555, 2001.
- [56] S. H. Chung, T. Allen, and S. Kuyucak, "Conducting-state properties of the KcsA potassium channel from molecular and Brownian dynamics simulations," *Biophys. J.*, vol. 82, pp. 628–645, 2002.
- [57] P. Jordan, "Semi-microscopic modeling of permeation through ion channels," *IEEE Trans. Nanobiosci.*, vol. 4, no. 1, pp. 94–101, Mar. 2005.
- [58] T. Allen, A. Bliznyuk, A. Rendell, S. Kuyucak, and S. H. Chung, "The potassium channel: Structure, selectivity and diffusion," *J. Chemical Phys.*, vol. 112, pp. 8192–8204, 2000.
- [59] S. Bernéche and B. Roux, "Molecular dynamics of the KcsA K⁺ channel in a bilayer membrane," *Biophys. J.*, vol. 78, pp. 2900–2917, 2000.
- [60] P. C. Biggin and M. S. Sansom, "Open-state models of a potassium channel," *Biophys. J.*, vol. 87, pp. 1867–1876, 2002.
- [61] S. Bernéche and B. Roux, "Energetics of ion conduction through the K⁺ channel," *Nature*, vol. 414, pp. 73–77, 2001.
- [62] J. Åqvist and V. B. Luzhkov, "Ion permeation mechanism of the potassium channel," *Nature*, vol. 404, pp. 881–884, 2000.
- [63] A. Burykin, M. Kato, and A. Warshel, "Exploring the origin of the ion selectivity of the KcsA potassium channel," *Protein Struct. Funct.*, vol. 57, pp. 412–426, 2003.
- [64] R. Mashl, Y. Tang, J. Schnitzer, and E. Jakobsson, "Hierarchical approach to predicting permeation in ion channels," *Biophys. J.*, vol. 81, pp. 2473–2483, 2001.
- [65] A. Burykin, C. Schutz, J. Villa, and A. Warshel, "Simulations of ion current realistic models of ion channels: KcsA potassium channel," *Proteins: Structure, Function and Genetics*, vol. 47, pp. 265–280, 2002.
- [66] B. Roux, "Ion conduction and selectivity," *Ann. Rev. Biophys. Biomol. Struct.*, vol. 34, pp. 153–171, 2005.
- [67] D. Tieleman, P. Beggan, G. Smith, and M. Sansom, "Simulation approaches to ion channel structure-function relationships," *Q. Rev. Biophys.*, vol. 34, pp. 473–561, 2001.
- [68] L. Cuello, J. Romero, D. Cortes, and E. Perozo, "pH dependent gating in the *streptomyces lividans* K⁺ channel," *Biochemistry*, vol. 37, pp. 3229–3236, 1998.
- [69] L. Heginbotham, M. LeMasurier, L. Kolmakova-Partensky, and C. Miller, "Single *Streptomyces lividans* K⁺ channels: Functional asymmetries and sidedness of proton activation," *J. General Physiol.*, vol. 114, pp. 551–559, 1999.
- [70] M. LeMasurier, L. Heginbotham, and C. Miller, "KcsA: It's a potassium channel," *J. General Physiol.*, vol. 118, pp. 303–313, 2001.
- [71] S. H. Chung, T. Allen, and S. Kuyucak, "Modeling diverse range of potassium channels with Brownian dynamics," *Biophys. J.*, vol. 83, pp. 263–277, 2002.
- [72] B. Corry, M. O'Mara, and S. H. Chung, "Conduction mechanisms of chloride ions in ClC-type channels," *Biophys. J.*, vol. 86, pp. 846–860, 2004.
- [73] C. Miller, "Open-state substructure of single chloride channels from *torpedo electroplax*," *Philosophical Trans. Roy. Soc. London*, vol. B299, pp. 401–411, 1982.
- [74] C. Fahlke, "Ion permeation and selectivity in ClC-type chloride channels," *Amer. J. Renal Physiol.*, vol. 280, pp. F748–F758, 2001.
- [75] A. Accardi and C. Miller, "Secondary active transport mediated by a prokaryotic homologue of ClC Cl⁻ channels," *Nature*, vol. 427, pp. 803–807, 2004.
- [76] W. Almers, E. W. McCleskey, and P. T. Palade, "A non-selective cation conductance in frog muscle blocked by micromolar external calcium ions," *J. Physiol.*, vol. 353, pp. 565–583, 1984.
- [77] A. Finkelstein, *Water Movement Through Lipid Bilayers, Pores and Plasma Membranes*. New York: Wiley-Interscience, 1987.
- [78] T. W. Allen, O. S. Andersen, and B. Roux, "Energetics of ion conduction through the gramicidin channel," *Proc. Nat. Acad. Sci. USA*, vol. 101, pp. 117–122, 2004.
- [79] H. R. Guy and S. R. Durell, "Structural models of Na⁺, Ca²⁺, and K⁺ channels," in *Ion Channels Diseases*. New York: Rockefeller Univ. Press, 1995.
- [80] G. M. Lipkind and H. A. Fozzard, "KcsA crystal structure as framework for a molecular model of the Na⁺ channel pore," *Biochemistry*, vol. 39, pp. 8161–8170, 2000.

- [81] B. Hille, "The permeability of the sodium channel to organic cations," *J. General Physiol.*, vol. 58, pp. 599–619, 1971.
- [82] S. H. Heinemann, H. Terlau, W. Stühmer, K. Imoto, and S. Numa, "Calcium channel characteristics conferred on the sodium channel by single mutations," *Nature*, vol. 356, pp. 441–443, 1992.
- [83] T. Schlieff, R. Schönherr, K. Imoto, and S. H. Heinemann, "Pore properties of the rat brain II sodium channels mutated in the selectivity filter domain," *Eur. Biophys. J.*, vol. 25, pp. 75–91, 1996.
- [84] Y. M. Sun, I. Favre, L. Schild, and E. Moczydlowski, "On the structural basis for size-selective permeation of organic cations through the voltage-gated sodium channel—Effect of alanine mutations at the DEKA locus on selectivity, inhibition by Ca^{2+} and H^+ , and molecular sieving," *J. General Physiol.*, vol. 110, pp. 693–715, 1997.
- [85] T. Vora, B. Corry, and S. H. Chung, "A model of sodium channels," *Biochimica et Biophysica Acta—Biomembranes*, vol. 1668, pp. 106–116, 2004.
- [86] J. Spall, *Introduction to Stochastic Search and Optimization*. New York: Wiley, 2003.
- [87] G. Pflug, *Optimization of Stochastic Models: The Interface Between Simulation and Optimization*. Reading, MA: Kluwer, 1996.
- [88] S. Andradottir, "Accelerating the convergence of random search methods for discrete stochastic optimization," *ACM Trans. Modelling Computer Simulation*, vol. 9, no. 4, pp. 349–380, Oct. 1999.
- [89] M. Alrefaei and S. Andradottir, "A modification of the stochastic ruler method for discrete stochastic optimization," *Eur. J. Operational Res.*, vol. 133, pp. 160–182, 2001.
- [90] V. Krishnamurthy, X. Wang, and G. Yin, "Spreading code optimization and adaptation in CDMA via discrete stochastic approximation," *IEEE Trans. Info Theory*, vol. 50, no. 9, pp. 1927–1949, Sept. 2004.
- [91] I. Berenguer, X. Wang, and V. Krishnamurthy, "Adaptive MIMO antenna selection via discrete stochastic optimization," *IEEE Trans. Signal Proc.*, vol. 53, no. 1, pp. 4315–4329, Nov. 2005.
- [92] V. Krishnamurthy and G. Yin, "Kernel based learning algorithms for single ion channels—Dynamic kinetic control of patch clamp for estimating equilibrium potential," *IEEE Trans. Nanobiosci.*, vol. 5, pp. 115–125, Jun. 2006.
- [93] J. Swisher, S. Jacobson, P. Hyden, and L. Schruben, "A survey of simulation optimization techniques and procedures," in *Proc. 2000 Winter Simulation Conf.*, Orlando, FL, 2000.
- [94] J. C. Gittins, *Multi-Armed Bandit Allocation Indices*. New York: Wiley, 1989.
- [95] S. Andradottir, "A method for discrete stochastic optimization," *Manage. Sci.*, vol. 41, no. 12, pp. 1946–1961, 1995.
- [96] S. Andradottir, "A global search method for discrete stochastic optimization," *SIAM J. Optimization*, vol. 6, no. 2, pp. 513–530, May 1996.
- [97] W. Gong, Y. Ho, and W. Zhai, "Stochastic comparison algorithm for discrete optimization with estimation," *SIAM J. Optimization*, vol. 10, no. 2, pp. 384–404, 1999.
- [98] D. Yan and H. Mukai, "Stochastic discrete optimization," *SIAM J. Control Optimization*, vol. 30, no. 3, pp. 594–612, 1992.
- [99] L. Shi and S. Olafsson, "An integrated framework for deterministic and stochastic optimization," in *Proc. 1999 Winter Simulation Conf.*, 1997, pp. 395–401.
- [100] S. Gelfand and S. Mitter, "Simulated annealing with noisy or imprecise energy measurements," *J. Optim. Theory Appl.*, vol. 62, pp. 49–62, 1989.
- [101] G. Yin, V. Krishnamurthy, and C. Ion, "Regime switching stochastic approximation algorithms with application to adaptive discrete stochastic optimization," *SIAM J. Optimization*, vol. 14, no. 4, pp. 117–1215, 2004.
- [102] V. Krishnamurthy and S. H. Chung, "Adaptive learning algorithms for nerst potential and current-voltage curves in nerve cell membrane ion channels," *IEEE Trans. Nanobiosci.*, vol. 2, no. 4, pp. 266–278, Dec. 2003.
- [103] S. Ross, *Simulation*, 3rd ed. New York: Academic, 2002.
- [104] H. Kushner and G. Yin, *Stochastic Approximation Algorithms and Recursive Algorithms and Applications*, 2nd ed. New York: Springer-Verlag, 2003.
- [105] V. Krishnamurthy, M. Hoyle, R. Saab, and S. H. Chung, "Permeation in gramicidin ion channels by directly estimating the potential of mean force using Brownian dynamics simulation," *J. Computational Theoretical Nanosci.*, vol. 3, pp. 702–711, 2006.
- [106] L. Schild, A. Ravindran, and E. Moczydlowski, " Zn^{2+} -induced subconductance events in cardiac Na^+ channels prolonged by batrachotoxin," *J. General Physiol.*, vol. 97, pp. 117–142, 1991.
- [107] L. Schild and E. Moczydlowski, "Permeation on Na^+ through open and Zn^{2+} -occupied conductance states of cardiac sodium channels modified by batrachotoxin: Exploring ion-ion interactions in a multi-ion channel," *Biophys. J.*, vol. 66, pp. 654–666, 1994.
- [108] R. J. French, J. F. W. III, W. F. Wonderlin, A. S. Kularatna, and B. K. Krueger, "Ion permeation, divalent ion block, and chemical modifications of single sodium channels," *J. General Physiol.*, vol. 103, pp. 447–470, 1994.
- [109] A. Singer and Z. Schuss, "Brownian simulations and uni-directional flux in diffusion," *Phys. Rev. E*, vol. 71, no. 026 115, 2005.
- [110] B. Nadler, A. Singer, and Z. Schuss, "Langevin trajectories between fixed concentrations," *Phys. Rev. Lett.*, vol. 94, no. 218 101, 2005.
- [111] M. Fernandes and J. de la Torre, "Brownian dynamics simulation of rigid particles of arbitrary shape in external fields," *Biophys. J.*, vol. 83, no. 6, pp. 3039–3048, 2002.

ABOUT THE AUTHORS

Vikram Krishnamurthy (Fellow, IEEE) was born in 1966. He received the B.S. degree from the University of Auckland, New Zealand, in 1988, and the Ph.D. from the Australian National University, Canberra, in 1992.

Since 2002, he has been a Professor and Canada Research Chair at the Department of Electrical Engineering, University of British Columbia, Vancouver, Canada. Prior to 2002, he was a chaired Professor in the Department of Electrical and Electronic Engineering, University of Melbourne, Australia, where he also served as Deputy Head of the department. His current research interests include stochastic modeling of biological ion channels, stochastic optimization and scheduling, and statistical signal processing. He is Coeditor (with S. H. Chung and O. Andersen) of the book *Biological Membrane Ion Channels—Dynamics Structure and Applications* (Springer-Verlag, 2006).

Dr. Krishnamurthy has served as Associate Editor for several journals including IEEE TRANSACTIONS ON SIGNAL PROCESSING, IEEE TRANSACTIONS AEROSPACE AND ELECTRONIC SYSTEMS, IEEE TRANSACTIONS ON CIRCUITS AND SYSTEMS B, IEEE TRANSACTIONS ON NANOBIOSCIENCE, and SYSTEMS AND CONTROL LETTERS.



Shin-Ho Chung received the B.Sc. degree from Stanford University, Stanford, CA, and London University, London, U.K., and the Ph.D. degree from Harvard University, Cambridge, MA.

He held a postdoctoral position at the Research Laboratory of Electronics, Massachusetts Institute of Technology, Cambridge. Currently, he is the Head of the Computational Biophysics Group in the Research School of Biological Sciences, Australian National University, Canberra. His primary research effort is aimed at building theoretical models of biological ion channels.

